General Circulation Model Simulation of the Semiannual Oscillation of the Tropical Middle Atmosphere

KEVIN HAMILTON

Atmospheric and Oceanic Sciences Program, Princeton University, Princeton, New Jersey

J. D. MAHLMAN

Geophysical Fluid Dynamics Laboratory/NOAA, Princeton University, Princeton, New Jersey

(Manuscript received 20 January 1988, in final form 13 May 1988)

ABSTRACT

A study has been made of the evolution of the zonal-mean zonal wind and temperature in a multiyear integration of the 40-level, 3° × 3.6° resolution "SKYHI" general circulation model (GCM) that has been developed at GFDL. In the tropical upper stratosphere the mean wind variation is dominated by a strong semiannual oscillation (SAO). The peak SAO amplitude in the model is almost 25 m s^{-1} and occurs near the 1 mb level. The phase of the SAO near the stratopause is such that maximum westerlies occur shortly after the equinoxes. These features are in good agreement with the available observations. In addition the meridional width of the stratopause SAO in the GCM compares well with observations.

A diagnostic analysis of the zonal-mean momentum balance near the tropical stratopause was performed using the detailed fields archived during the GCM integration. It appears that the easterly accelerations in the model SAO are provided by a combination of (i) divergence of the meridional component of the Eliassen–Palm flux associated with quasi-stationary planetary waves and (ii) mean angular momentum advection by the residual meridional circulation. The effects of the residual circulation dominate in the summer hemisphere, while the eddy contributions are more important in the winter hemisphere. The westerly accelerations in the model SAO result from the convergence of the vertical momentum transport associated with gravity waves that have a broad distribution of space and time scales. Thus, in contrast to some simple theoretical models, large-scale equatorial Kelvin waves appear to play only a very minor role in the dynamics of the SAO in the SKYHI GCM.

A second equatorial SAO amplitude maximum was found in the tropical upper mesosphere of the GCM. This apparently corresponds to the mesopause SAO that has been identified in earlier observational studies. While the observed phase of this oscillation is reproduced in the model, the simulated amplitude is unrealistically small.

The model integration included the computation of the concentration of N_2O. The results show a fairly realistic simulation of the semiannual variation of tropical stratospheric N_2O mixing ratio seen in satellite observations.

1. Introduction

The variations in the prevailing zonal wind in the tropical stratopause region are known to include a strong semiannual oscillation (SAO). This SAO has been documented in numerous studies of tropical rocketsonde wind measurements (Reed 1965, 1966; Angell and Korshover 1970; Belmont et al. 1974; Hopkins 1975; Hirota 1978; Hamilton 1982a). As an example, Fig. 1 (adapted from Hamilton 1982a) shows a height–time section of the climatological monthly mean zonal wind at Kwajalein between 12.2 and 0.01 mb (about 30 and 80 km). Near the 1 mb level the SAO is quite evident, with maximum easterlies occurring in January and August, and maximum westerlies in March and October. Above about 0.2 mb (~60 km) the SAO is clearly much weaker than the annual variation, but at still higher levels near the mesopause (~0.01 mb or 80 km) the strong SAO reappears. As noted by Hirota (1978) and Hamilton (1982a) the mesopause SAO is roughly 180° out of phase with the stratopause oscillation.

Given the strong semiannual component of radiative forcing at low latitudes, the existence of a strong SAO in this region may not be surprising. However, the observed SAO has a number of interesting features that require theoretical explanations, such as the strong super-rotation of the equatorial flow in the westerly phase (a puzzling aspect when the SAO was first discovered; e.g., Reed 1966), and the downward propagation of

Corresponding author address: Dr. Kevin Hamilton, NOAA/GFDL, Princeton University, P.O. Box 308, Princeton, NJ 08542.

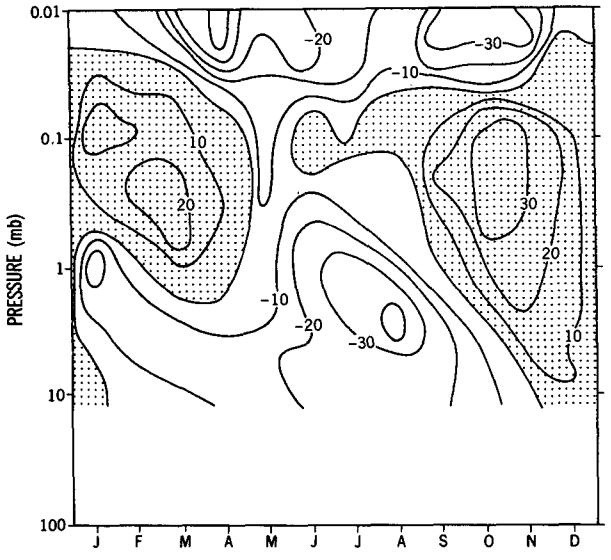

FIG. 1. Time–height section showing average zonal winds for each month of the year determined from several years of rocketsonde observations at Kwajalein (8.7°N, 167.7°E). The contour interval is 10 m s^{-1} and shading denotes westerly winds. Results above 3 mb based on the data discussed in Hamilton (1982a), below 3 mb on the data of Cayford and Hamilton (1987).

the westerly wind accelerations (similar to those seen in the quasi-biennial oscillation in the lower stratosphere).

Unfortunately, the SAO occurs in a part of the atmosphere where the detailed dynamics are particularly difficult to study. The upper stratosphere and mesosphere have only very sparse direct wind observations. This problem is aggravated by the difficulty in inferring winds from satellite-derived temperature observations at low latitudes. Detailed diagnostic studies of the momentum budget of the SAO are not possible with currently available observations. Thus it is not surprising that studies of the SAO dynamics have tended to employ simple mechanistic models (e.g., Meyer 1970; Dunkerton 1979; Holton and Wehrbein 1980; Takahashi 1984a,b) or to be based on rather indirect diagnostic inferences (Hamilton 1986; Hitchman and Leovy 1988).

Another possible approach to the study of the SAO dynamics is the analysis of simulations produced by comprehensive general circulation models (GCMs). Thus far the only published GCM results showing a fairly realistic SAO appear to be those from the 40-level Geophysical Fluid Dynamics Laboratory troposphere–stratosphere–mesosphere model (referred to as the "SKYHI" model). In particular, the results for the tropical middle atmosphere obtained with rather low horizontal resolution versions of the model have been briefly discussed by Mahlman and Sinclair (1980) and Mahlman and Umscheid (1984). The present paper is a much more detailed analysis of the dynamics of the SAO as simulated in a long integration of a higher resolution version of this model.

A brief review of observations and theoretical models of the SAO is presented in section 2. A summary of the relevant features of the SKYHI GCM is given in section 3. Section 4 discusses the results for the SAO in the simulated zonal mean winds and temperatures. Section 5 considers the transformed-Eulerian mean zonal momentum balance in the model's stratopause SAO. Section 6 is a more detailed discussion of the role of wave-driving in the simulated SAO. Section 7 is a brief examination of the dynamics of the mesopause SAO in the model. Section 8 discusses the effects of the SAO on the simulated distribution of a passive trace constituent (N_2O). The conclusions are summarized in section 9.

2. Brief review of observations and theory of the SAO

The basic features of the stratopause SAO in the zonal wind were apparent in Reed's early analysis of rocketsonde observations (Reed 1965, 1966). In particular, Reed found that the zonal wind at the tropical stratopause evolves so that easterly maxima of roughly 25–30 m s^{-1} occur shortly after the solstices, and westerly maxima of comparable magnitude just after the equinoxes. The precise timing of the wind variations depends on height, with later phases occurring at lower levels. There is a strong asymmetry in this respect between the easterly and westerly acceleration regimes. The westerly accelerations seem to propagate downward in a fairly regular manner, while the easterly accelerations appear almost simultaneously at all altitudes (see Fig. 1). Observations of the zonal wind at several stations reveal a stratopause SAO that is basically trapped along the equator, although there is an indication of slightly larger amplitudes just south of the equator than north of the equator (e.g., Hopkins 1975). The wind SAO is accompanied by a SAO in temperature that can be conveniently observed by satellite radiometers (Barnett et al. 1985; Hitchman and Leovy 1986; Gao et al. 1987). The satellite data suggest that the SAO is very nearly zonally-symmetric (Gao et al. 1987).

The occurrence of super-rotation of the equatorial winds during the westerly phase of the SAO has naturally suggested the presence of a vertical eddy transport of westerly momentum into the tropical upper stratosphere (e.g., Holton 1975; Hirota 1978). The observational analysis of Hirota (1978) showed the presence of Kelvin waves with phase speeds ~50–70 m s^{-1} in the tropical upper stratosphere (see also Salby et al. 1984). Hirota suggested that these Kelvin waves could provide the momentum transport necessary to explain the westerly accelerations in the SAO. This idea has been incorporated into simple SAO models by Dunkerton (1979), Takahashi (1984a,b), and Gray and Pyle (1987).

While vertical eddy momentum transports appear to be implicated in the generation of westerly SAO accelerations, there are other possible mechanisms for producing the easterly accelerations. Reed (1966) suggested that advection of the summer hemisphere mean easterlies across the equator by the mean meridional circulation could account for tropical easterly maxima around the time of the solstices. This mechanism was shown to account for reasonably good simulations of the easterly phase of the SAO found in some simple zonally-symmetric models (Holton and Wehrbein 1980; Hamilton 1981) and in a low-resolution GCM (Mahlman and Sinclair 1980).

Another possibility for the generation of the easterly phase of the SAO was proposed by Hirota (1978, 1980; see also Hopkins 1975). Hirota attributed the easterly mean flow accelerations to the effects of meridional momentum transports associated with large-scale quasi-stationary planetary waves generated in the extratropics.

As noted in the Introduction, it is impossible at present to conduct a detailed diagnostic study using real data to identify conclusively the forcing mechanisms for the SAO. Hamilton (1986) attempted a rather indirect investigation of SAO dynamics based on observations. In particular he computed the residual meridional circulation using diabatic heating rates obtained by inserting observed temperatures into a sophisticated numerical radiative transfer model. He then used this calculated residual circulation, together with the observed mean flow accelerations, to estimate the wave-driving of the mean flow required to balance the momentum budget. He then interpreted the meridional profile of the inferred wave-driving in the light of current wave–mean flow interaction theory. In particular Hamilton found that the wave-driving could be imagined as being composed of an equatorially-centered westerly component plus an easterly component that is large in the winter hemisphere subtropics and decreases as one moves into the equatorial region. Hamilton interpreted the first component as being due to equatorial Kelvin waves, and the second as being associated with large-scale planetary waves of extratropical origin. An implication of this interpretation is that the easterly SAO accelerations on the winter side of the equator are to be largely attributed to Hirota's mechanism, while on the summer side they are mainly due to the effects of the residual meridional circulation (as proposed by Holton and Wehrbein 1980, and Mahlman and Sinclair 1980).

Hitchman and Leovy (1988) have attempted to use satellite-derived temperature analyses to estimate the amplitude of planetary-scale Kelvin waves, and hence their contribution to the zonal-mean momentum balance in the tropical stratosphere and mesosphere. They concluded that a significant fraction ($\sim$20%–70%) of the observed westerly mean flow acceleration in the SAO can be ascribed to the effects of Kelvin waves with zonal wavenumbers 1–3. They suggested that the remaining westerly forcing may be produced by dissipation of small-scale vertically-propagating gravity waves.

The results to be discussed in the present paper will demonstrate that the GFDL SKYHI GCM does produce a fairly realistic simulation of the stratopause SAO. The simulation will be analyzed in detail to address the issues raised in earlier observational and modelling studies. In particular, in the model it is possible to compute accurately the relative contributions of the eddy forcing and the residual circulation to the mean flow acceleration. The model data also allows the determination of the spatial and temporal scales of the waves responsible for the eddy forcing of the mean flow. Through the diagnostic analysis a rather complete picture can be obtained of the operation of the stratopause SAO in the GCM.

Analysis of the relatively infrequent mesospheric rocket soundings at Ascension Island (8°S; Hirota 1978) and Kwajalein (8.7°N; Hamilton 1982a) show the existence of another SAO at upper mesospheric/lower thermospheric levels. This oscillation has approximately the same maximum amplitude as the stratopause SAO, but is roughly 180° out of phase. Dunkerton (1982) suggested that the mesopause SAO might be explained by the effects of small-scale gravity waves on the equatorial mean winds. In particular, he argued that vertically propagating waves with easterly (westerly) phase speeds should be filtered out at stratospheric levels during the (easterly) westerly phase of the stratopause SAO. If the remaining waves break in the upper mesosphere, then one can anticipate a wave-driving of the mesopause winds that will be roughly out of phase with the stratopause SAO.

As shown below, the SKYHI GCM produces a mesospheric SAO similar in some respects to that observed. However, the simulation of the mesopause SAO is much less realistic than that of the stratopause SAO. In particular, the mesopause SAO in the model is less than one-half as strong as that observed. Also the annual-mean wind in the model's tropical upper mesosphere is quite unrealistic in the GCM. Thus less attention is paid in this paper to diagnosing the detailed driving mechanisms for the mesopause SAO. However, section 7 does briefly discuss how the limitations of the model formulation may account for the relatively poor simulation of the tropical upper mesosphere.

3. Description of the GCM

The "SKYHI" GCM is a numerical model designed for comprehensive, time-dependent simulation of the dynamics of the global troposphere, stratosphere and mesosphere. The basic description of the model is given in Fels et al. (1980), and earlier results obtained have been discussed in Mahlman and Sinclair (1980), An-

drews et al. (1983), Hayashi et al. (1984), Mahlman and Umscheid (1984, 1987) and Miyahara et al. (1986). Only a very brief summary of the important features of the model will be given below.

The GCM has 40 levels extending from the ground to about 0.01 mb (~80 km). The governing equations are discretized on a regular latitude–longitude grid. The model has now been run at four different horizontal resolutions 9° × 10°, 5° × 6°, 3° × 3.6° and 1° × 1.2° (thus far only a half-year of the 1° × 1.2° simulation has been completed, and so the results are not yet applicable to the present problem). The model is formulated in a vertical coordinate that approximates the standard σ system in the lower atmosphere and is identical to isobaric coordinates above 354 mb. The vertical resolution decreases gradually with height; in the upper stratosphere there is roughly 2.5 km separation between levels, while at the top of the model the level spacing is roughly 6 km.

As an upper boundary condition the isobaric vertical velocity, ω, is set to zero at zero pressure. In an attempt to reduce spurious wave reflection from the upper boundary, an eddy Newtonian cooling term is added to the thermodynamic equation and an eddy Rayleigh friction is added to the horizontal momentum equations at the top level.

The model was run with seasonally varying solar insolation and (specified) sea surface temperatures. No diurnal cycle of solar radiation was included, however. Realistic longwave and shortwave radiative heating rates were computed every six hours using a specified distribution of clouds. Parameterizations are included for various subgrid-scale processes (e.g., moist convective adjustment). Of particular interest for the present paper is a parameterized Richardson number-dependent vertical mixing of heat and momentum (see Fels et al. 1980).

The simulated data to be analyzed in this paper represent part of a five-year integration of the 3° × 3.6° version of the model. This integration began in October using initial conditions interpolated from a multiyear, seasonally marched integration of the 5° × 6° version of the model. In the actual solar astronomy dating system used at GFDL, the higher-resolution model integration began on astronomical date 1 October "1982." The results of the integration for the three year period from July "1983" through June "1986" were analyzed in the present project. Throughout most of this period "snapshots" of the model fields were saved to tape once each day. During the period 15 December "1983" through 23 March "1984" all of the variables were saved twice a day, and the wind and temperature fields were saved every two hours.

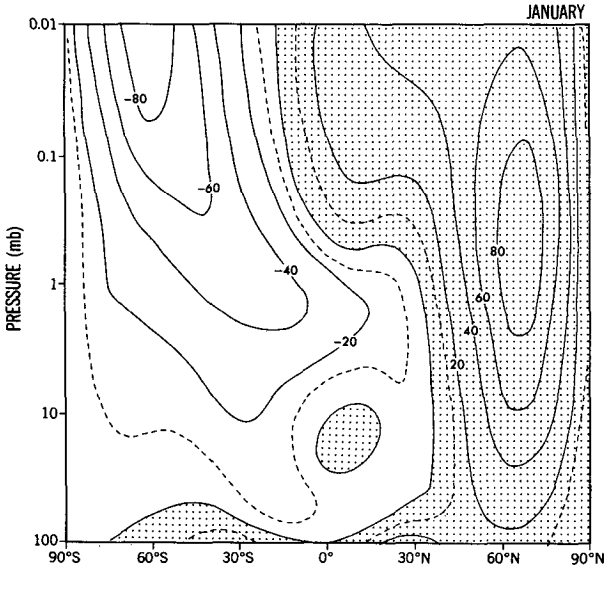

FIG. 2. Zonal-mean zonal wind averaged over January "1984," "1985" and "1986." The interval between solid contours is 20 m s^{-1} and regions of mean westerlies are shaded. The dashed contours are for ±10 m s^{-1}.

4. Results for the zonal-mean zonal wind and temperature

Figures 2–5 show meridional cross sections of the zonally averaged zonal wind, $\bar{u}$, above 100 mb for the three year means in January, April, July and October. Outside of the equatorial region these figures can be compared to the geostrophic wind observations shown in Hamilton (1982b,c), Geller et al. (1983) and Barnett and Corney (1985). In common with most other GCMs, the simulated polar night jets in the winter hemisphere are stronger and are located farther poleward than those actually observed. This problem is particularly severe in the Southern Hemisphere during July (Fig. 4); in this month the simulated jet strength is greater than 160 m s^{-1}, far in excess of the 103 m s^{-1} maximum $\bar{u}$ reported for July by Barnett and Corney (1985, their values are for the geostrophic wind which is presumably somewhat stronger than the actual $\bar{u}$). The simulated easterly jets in the summer hemisphere are in reasonably good agreement with observations (although displaced rather too far poleward), except in the upper mesosphere (above about 0.05 mb). In this high altitude region the observations suggest that the easterly jet closes off and weakens quickly with height, whereas the simulated easterlies continue to increase right up to the highest model level. In this context it should be noted that the model does not include any parameterization of the drag effects due to unresolved gravity wave motions.

The simulated $\bar{u}$ field in April (Fig. 3) is in reasonable agreement with observations, although the Southern Hemisphere westerly jet in the model is somewhat too strong and located too far poleward. The simulated westerly jets in October are realistic, except above about 5 mb in the Southern Hemisphere. In this region observations suggest a sharp decrease in the jet strength

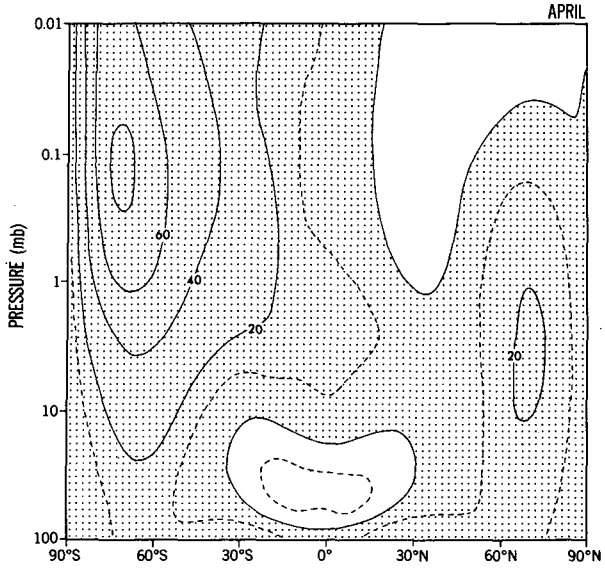

FIG. 3. As in Fig. 2, but for April.

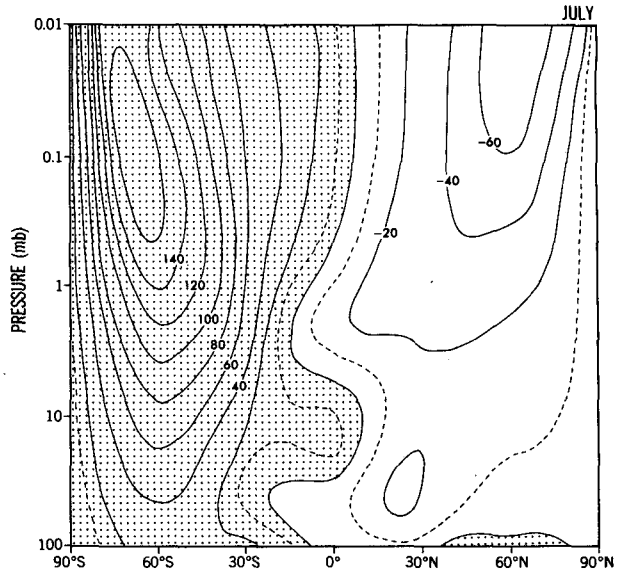

FIG. 4. As in Fig. 2, but for July "1983," "1984" and "1985."

with altitude, with weak easterlies filling most of the mesosphere. By contrast, the model has quite strong westerlies in this part of the atmosphere.

The general picture that emerges is of a model simulation with fairly realistic extratropical zonal-mean wind structure, but with the model generally displaying jets that are too strong. These strong jets are associated with enhanced equator-to-pole temperature contrasts in the model. The obvious implication is that the eddy fluxes in the GCM are too weak, so that the model develops a temperature structure that is somewhat too close to radiative equilibrium. This problem was shared to a much more acute degree by the lower resolution versions of the SKYHI model (Mahlman and Sinclair 1980; Mahlman and Umscheid 1984), and appears to be substantially alleviated in the very high 1° × 1.2° version (Mahlman and Umscheid 1987).

The winds in the equatorial region shown in Figs. 2–5 display a clear stratopause SAO, with the summer hemisphere easterlies extending across the equator in January and July, and the appearance of westerlies at the equatorial stratopause in April and October. The general pattern is similar to that seen in climatologies based on rocket observations (e.g., Murgatroyd 1969; CIRA 1972). The principal deficiency in the simulated equatorial winds occurs in the upper mesosphere, where the model produces weak westerlies while the observations (e.g., CIRA 1972) show strong mean easterlies. This problem may be due to the lack of thermally forced tides in the model, since the tides are thought to produce an intense easterly mean flow driving near the tropical mesopause (Miyahara 1978a,b; Hamilton 1981).

Figure 6 shows a time–height section of the monthly-average, zonal-mean zonal wind at the equator for the full three years of simulation. One striking aspect of this figure is the very small interannual variability evident in the lower stratosphere (where the real atmospheric circulation is dominated by the quasi-biennial oscillation). This lack of a quasi-biennial oscillation is shared by all other comprehensive GCMs. No definitive explanation for this deficiency in GCMs is currently available (although there have been speculations that the problem results from either inadequate vertical resolution or a too strong damping of the mean flow by subgrid scale processes in the models; e.g., see Plumb 1977; Hamilton 1981; Plumb and Bell 1982).

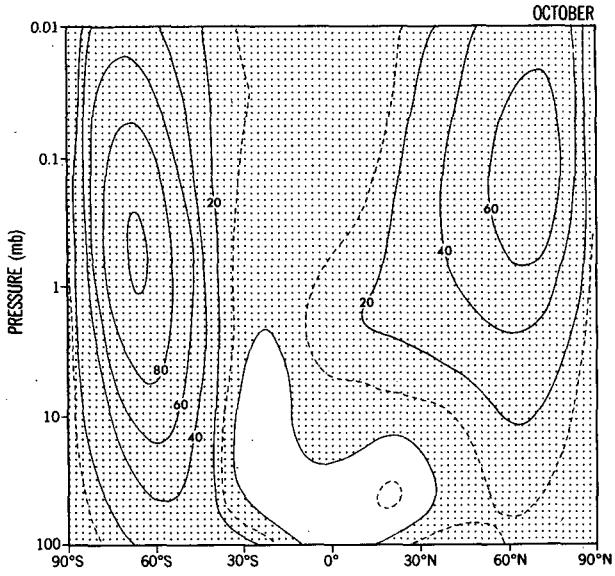

FIG. 5. As in Fig. 4, but for October.

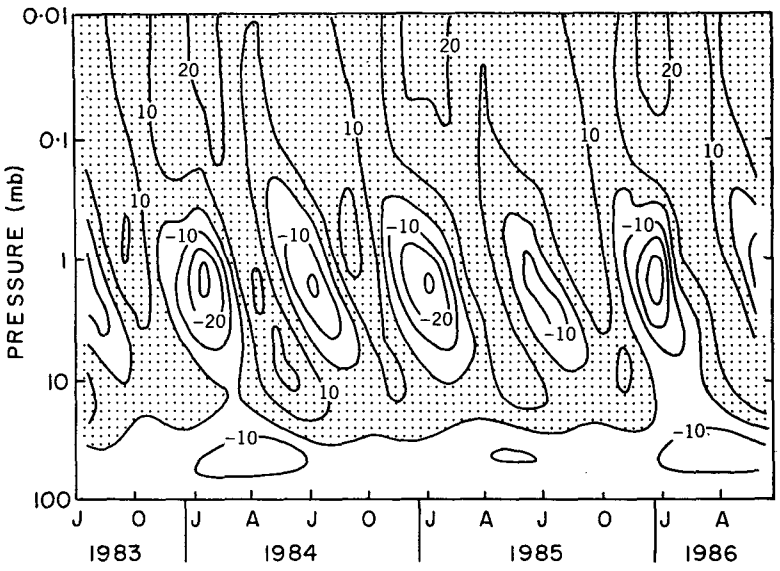

FIG. 6. Height–time section of the monthly-averaged zonal-mean zonal wind at the equator during three years of model simulation. The equatorial winds are estimated as the average of those at 1.5°S and 1.5°N. The contour interval is 10 m s^{-1} and shading indicates westerly winds.

By contrast, the simulation in the equatorial upper stratosphere and lower mesosphere is impressively realistic. The semiannual oscillation is clearly well developed in the vicinity of the stratopause, with maximum easterlies at the 1 mb level in January and July, and maximum westerlies in April and October. The first easterly and westerly maxima in each year seem to be somewhat larger than the second, in agreement with observations (Delisi and Dunkerton 1988). In contrast to the observations, however, both the westerly and easterly acceleration phases appear to display a gradual downward phase propagation.

The equatorial winds in the upper mesosphere displayed in Figs. 6 show the westerly bias relative to observations that was noted earlier. However, there is some evidence of the mesopause SAO in the model, since the strongest westerlies occur in both January and July. The peak-to-peak amplitude of this variation appears to be between 10 and 20 m s^{-1}, i.e. considerably less than actually observed.

Figure 7 shows the meridional cross section of the amplitude of the semiannual harmonic of the $\bar{u}$ variation determined from the monthly mean values throughout the three years of model simulation. The maximum near the equatorial stratopause is very evident. There is a slight tendency for the SAO to be stronger in the Southern Hemisphere than in the Northern Hemisphere (at least equatorward of 15°). This apparent asymmetry is rather more pronounced in observational SAO cross sections that have been published (e.g., Belmont et al. 1974; Hopkins 1975). However, it is important to remember that the observational estimates of the asymmetry near the equator have been largely based on rocket data from just three stations (Kwajalein, 8.7°N, Ft. Sherman, 9°N, and Ascension Island, 8°S).

The observations of Hopkins (1975) indicate a maximum amplitude for the zonal wind SAO of just over 25 m s^{-1}, while the model results in Fig. 7 show

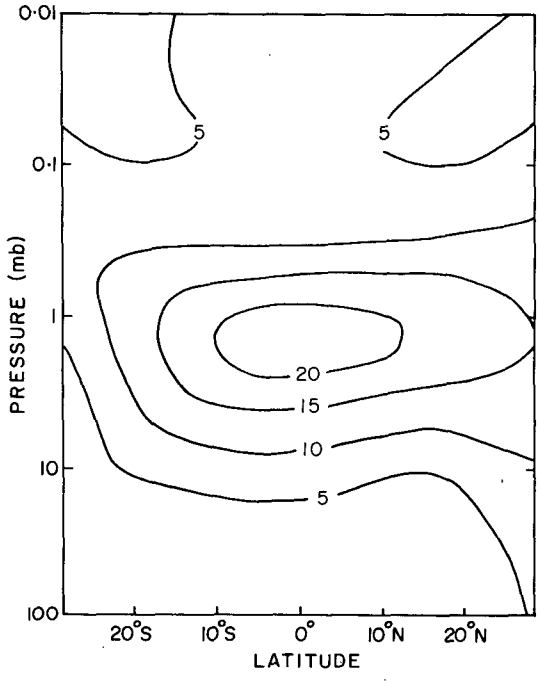

FIG. 7. Contours of the amplitude of the semiannual harmonic of the zonally-averaged zonal wind. Contour labels are in m s^{-1}.

a slightly smaller maximum amplitude. The largest amplitudes are just below the 1 mb level. The meridional width of the SAO indicated in Fig. 7 is similar to, but slightly less than that seen in the observed cross-sections. The amplitude of the $\bar{u}$ SAO in the upper mesosphere of the model is less than 10 m s^{-1}, contrasting with the roughly 20 m s^{-1} that has been observed (Hirota 1978; Hamilton 1982a).

Figure 8 displays the phase of the semiannual harmonic of the zonal wind variation in the model. The results show a very regular downward propagation of the SAO over almost the whole equatorial middle atmosphere. There is also a slight indication of phase propagation outward from the equator, at least at altitudes above 1 mb. These features are in good agreement with the observations of Hopkins (1975). The main discrepancy with observations is in the region below about 5 mb (~40 km); here the model results show a continuing downward propagation, in contrast to the roughly constant phase found in the rocket data (Hopkins 1975).

Figure 9 shows the amplitude of the semiannual harmonic of zonally averaged temperature, $\bar{T}$, in the three years of model simulation. This can be compared with results based on temperatures retrieved from satellite radiometer data shown in Fig. 10 (redrafted using the data in Barnett et al. 1985). The model results near the stratopause are in good agreement with observations, with maximum amplitudes in each case of just over 4°C. The model $\bar{T}$ SAO may be very slightly narrower in latitude than that observed, and the peak amplitude in the GCM occurs slightly lower than in the observations. However, the overall agreement for the

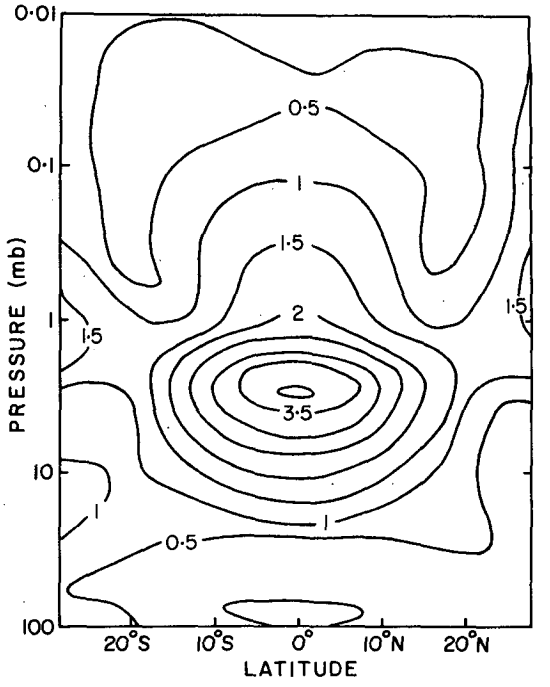

FIG. 9. Amplitude of the semiannual harmonic of the zonally-averaged temperature in the model. Contour labels in °C.

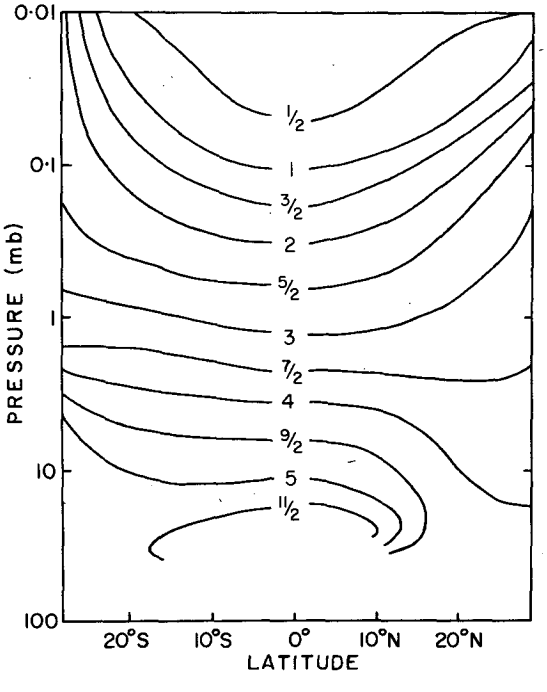

FIG. 8. Phase of the semiannual harmonic of the zonal-mean zonal wind. The contour labels give the time of the maximum westerlies associated with the SAO, in months after 1 January.

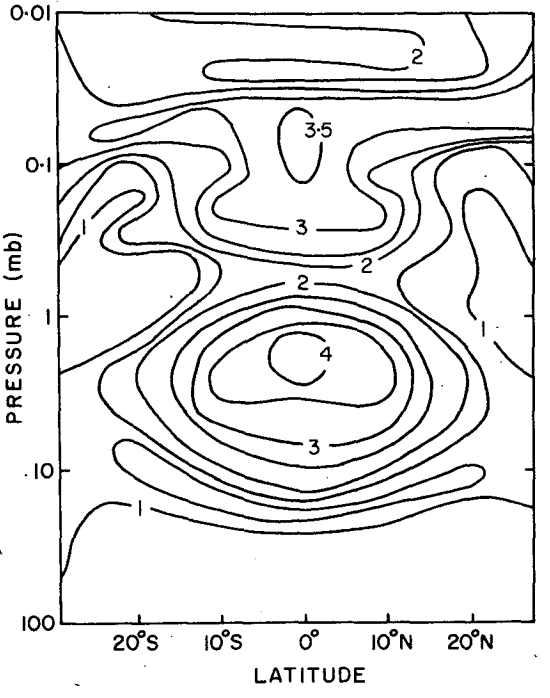

FIG. 10. As in Fig. 9, but for the satellite-based observational analysis of Barnett et al. (1985).

stratopause SAO is impressive (although it should be noted that the use of radiometer data with limited vertical resolution would be expected to somewhat suppress the observational estimates of the amplitude).

The phase of the semiannual harmonic of $\bar{T}$ in the model (not shown) displays regular downward phase propagation near the equator (similar to that seen for the $\bar{u}$ SAO in Fig. 8). There is a large phase shift between the equatorial and subtropical regions in the $\bar{T}$ SAO (a phase shift of between about 90° and 180°, depending on altitude). These features are just those expected for a temperature SAO that is in approximate thermal wind balance with the $\bar{u}$ SAO shown in Figs. 7 and 8.

The model results in Fig. 9 diverge quite noticably from the observations above about 0.5 mb. In particular, the observed $\bar{T}$ SAO amplitude grows strongly with height between about 0.5 and 0.08 mb, while the model results display a gradual decline in the amplitude throughout the mesosphere. The smallness of the temperature SAO in the model mesosphere is consistent with the weakness of the mesospheric wind SAO noted above.

In summary, it appears that the SKYHI GCM with 3° × 3.6° horizontal resolution produces a quite realistic simulation of the SAO in the zonally averaged flow in the vicinity of the tropical stratopause. The good quality of this simulation justifies the more detailed analysis of the dynamics of the model's SAO that is presented in the following sections. By contrast, there are serious deficiencies in the model simulation of the mesospheric SAO (as well as the annual mean winds in the tropical upper mesosphere).

5. Zonal-mean momentum balance

The model variables (including subgrid scale terms) at all grid points and levels are normally archived once per day. Since the SKYHI model integration involves the explicit solution of the zonal momentum and thermodynamic equations on pressure surfaces (above 354 mb), the numerics were formulated so that the usual isobaric zonal-mean zonal momentum and heat balances are satisfied "exactly" (i.e., to the roundoff precision of the computer). As shown in Andrews et al. (1983) the archived variables can be used to construct "exact" isobaric transformed-Eulerian (TE) momentum balances as well. In this section the diagnosed TE balances near the tropical stratopause in the model simulation will be presented, with a view to explaining the mechanisms responsible for the SAO.

One difficulty that arises in using the archived data is related to the once-per-day sampling. The model fields have so much high-frequency and small-scale variability at upper stratospheric/mesospheric levels that instantaneous values of a quantity like the acceleration of the zonal-mean zonal wind can have a very noisy meridional profile. Even when a "monthly mean" is computed as an average of 30 of these instantaneous snapshots, some of this small-scale variability in the spacial structure of the $\partial\bar{u}/\partial t$ field remains. It turns out that application of a simple 1–2–1 smoothing across successive latitude rows produces a reasonably smooth meridional profile of "monthly mean" $\partial\bar{u}/\partial t$. It appears that this smoothed profile is generally a better approximation to the profile of the true monthly mean of the acceleration (which can be computed from a knowledge of the actual $\bar{u}$ saved at the beginning and end of each month). It seems reasonable that this smoothing would also improve the results for the other components of the TE momentum balance. Thus all the profiles of the various terms in the momentum balance presented below have been 1–2–1 smoothed in latitude.

Figure 11 shows the terms in the TE momentum equation (e.g., equation 2.7 of Andrews et al. 1983) at the 1.08 mb level averaged over the three simulated February months. The "*CIRCULATION" term is the contribution to the mean flow acceleration from the vertical and horizontal advection of angular momentum associated with the residual meridional circulation. "EPFD" is the contribution to the mean flow acceleration from the divergence of the EP flux associated with the resolved eddies in the model. "DIFFUSION" is the contribution from the parameterized subgrid scale momentum diffusion. The actual zonal-

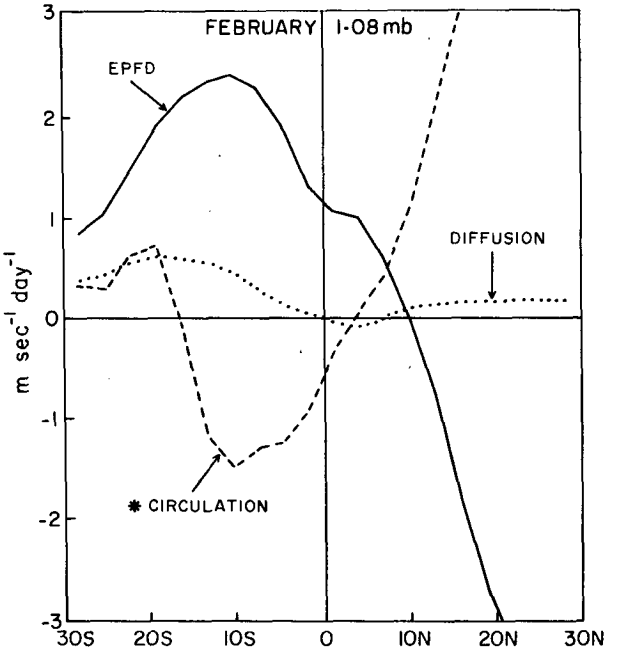

FIG. 11. Components of the transformed-Eulerian zonal-mean momentum balance at the 1.08 mb level in the model. Results are averages over February "1984," "1985" and "1986." The curve marked "*CIRCULATION" represents the contribution of the residual mean meridional circulation. The curve labelled "EPFD" is the zonal force/unit mass associated with the EP flux divergence of the eddies. "DIFFUSION" is the contribution from the parameterized subgrid scale mixing.

mean zonal wind acceleration (not shown) is obtained simply as the sum of these three terms (thus, for example, in Fig. 11 the sum of the terms is clearly positive at low latitudes, reflecting the fact that February is in the westerly acceleration phase of the stratopause SAO).

One striking point about Fig. 11 (and succeeding figures showing the same quantities) is that the "diffusion" term is generally small (typically 20% or less of the EPFD term). This is a comforting result, since in the lower resolution versions of the SKYHI model (Mahlman and Sinclair 1980; Mahlman and Umscheid 1984) the subgrid-scale momentum diffusion played a significant role in the dynamics of the simulated SAO. Equally reassuring is the diagnosis of the relative contributions of the vertical and horizontal components of the parameterized momentum diffusion in the present version of the model. The result (not shown) is that the convergence of the vertical component is typically five to ten times larger than that of the horizontal component. Thus the subgrid-scale horizontal momentum transport is a negligible factor in the dynamics of the stratopause SAO in the 3° × 3.6° resolution GCM.

The February results shown in Fig. 11 have a number of interesting features. At most latitudes there is an apparent tendency for the effects of the residual circulation to oppose those of the wave driving. This compensation was noted earlier by Andrews et al. (1983) in an analysis of an earlier version of the model. However, at low latitudes the compensation is far from perfect, and the $\partial\bar{u}/\partial t$ can actually be comparable in magnitude to the eddy driving itself. The overall pattern of the eddy forcing seen in Fig. 11 agrees well with the observationally-based inferences of Hamilton (1986). There is westerly wave-driving at the equator and in the summer hemisphere and easterly wave-driving poleward of about 12° in the winter hemisphere. The effects of the residual circulation can be divided into those due to meridional advection and vertical advection. The results (not shown) demonstrate that the effect of vertical advection, at least at the stratopause level, is rather small (typically less than 20% of the horizontal advection). The model's residual circulation in February (not shown) has strong ($\sim$0.5 m s^{-1}) flow at the stratopause from the Southern Hemisphere into the Northern Hemisphere. This produces an easterly mean flow forcing at the equator in the manner described by Holton and Wehrbein (1980) and Mahlman and Sinclair (1980). Thus in the westerly acceleration phase of the SAO the westerly wave-driving at the equator must fight this easterly forcing as well as account for the actual acceleration of the mean wind.

Figure 12 shows the same terms in the TE momentum balance averaged over the three August months in the simulation. The general pattern is similar to that seen in February, but with the Northern and Southern hemispheres interchanged. Thus, in August, there is a

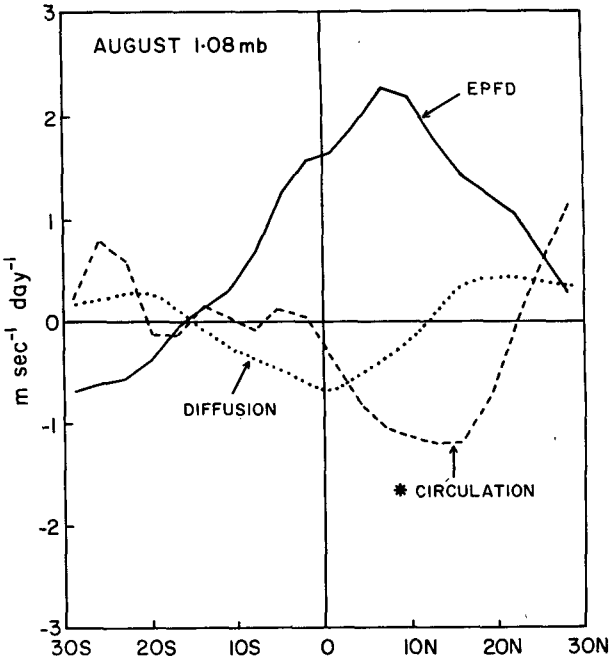

FIG. 12. As in Fig. 11, but for August.

westerly maximum in EP flux divergence displaced somewhat into the summer hemisphere. Also apparent is an easterly mean flow driving from the residual circulation at the equator and on the summer side of the equator. The most striking differences between Figs. 11 and 12 are in the winter hemisphere where in February both the easterly wave-driving and the effects of the residual circulation are much stronger than in August. This is consistent with the weaker planetary wave activity expected in austral winter than boreal winter. The weakness of the waves presumably leads to a temperature structure closer to radiative equilibrium (and thus a weaker residual circulation) in austral winter.

Figures 13 and 14 show the TE balance at 1.08 mb during November and May (i.e., near the maximum easterly SAO accelerations). It can be seen that the easterly acceleration on the autumn side of the equator is largely provided by the effects of the residual circulation, while on the spring side easterly wave-driving is important. Thus it appears that both the Holton–Wehrbein/Mahlman–Sinclair mechanism and Hirota's mechanism are important in producing the easterly acceleration phase of the SAO. In light of these results, it is not surprising that the easterly phase of the SAO has been found to be poorly developed on the winter side of the equator in zonally symmetric models (Holton and Wehrbein 1980; Hamilton 1981) or low-resolution GCMs which are strongly deficient in planetary wave activity (Mahlman and Sinclair 1980).

The diagnostic observational analysis of Hamilton (1986) produced estimates of the meridional structure of the EP flux divergence that are quite similar to those

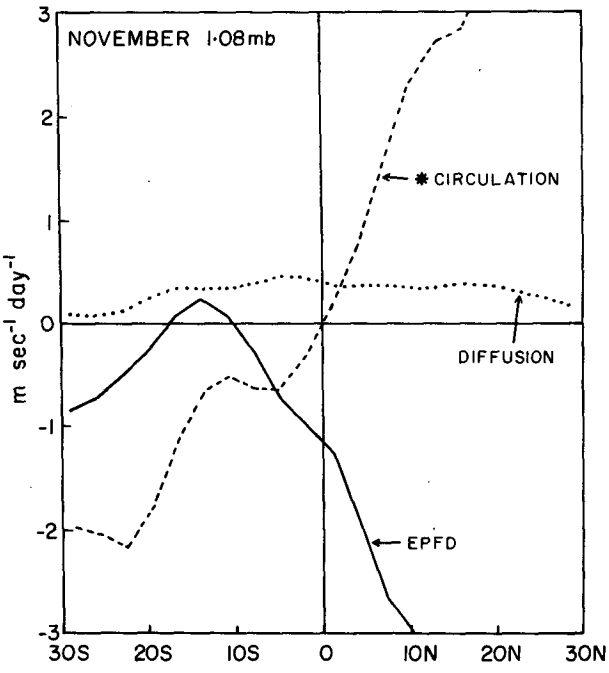

FIG. 13. As in Fig. 11, but for November.

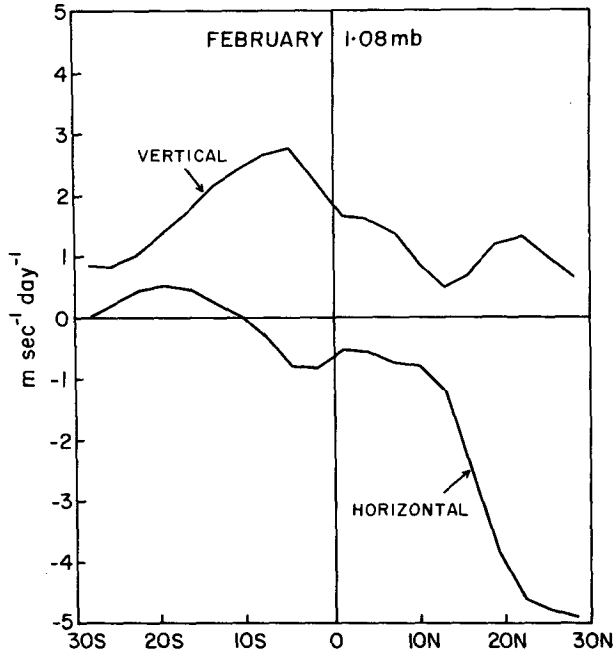

FIG. 15. Zonal force/unit mass due to the divergence of the vertical component of the EP flux, and that associated with the divergence of the horizontal component. Results for the 1.08 mb level and averaged over three Februaries.

found in the present model simulation, particularly in February. Hamilton interpreted his results for the total wave-driving as being the sum of two components: a (roughly) equatorially trapped westerly contribution attributable to a vertically propagating Kelvin wave, and an easterly contribution from meridional propagation of planetary waves that is strong in the subtropics of the winter hemisphere and decreases toward the equator. This interpretation can be tested more thoroughly in the GCM results. Figure 15 shows the decomposition of the total EP flux divergence at 1.08 mb in February into that due to the vertical and horizontal EP flux components. The results show that the vertical EP flux does indeed act to produce an equatorially centered westerly mean flow forcing, while the profile of the divergence of the horizontal EP flux is just as inferred by Hamilton (1986). Similar results (although with much weaker easterly EP flux in the winter hemisphere) are obtained for August (Fig. 16).

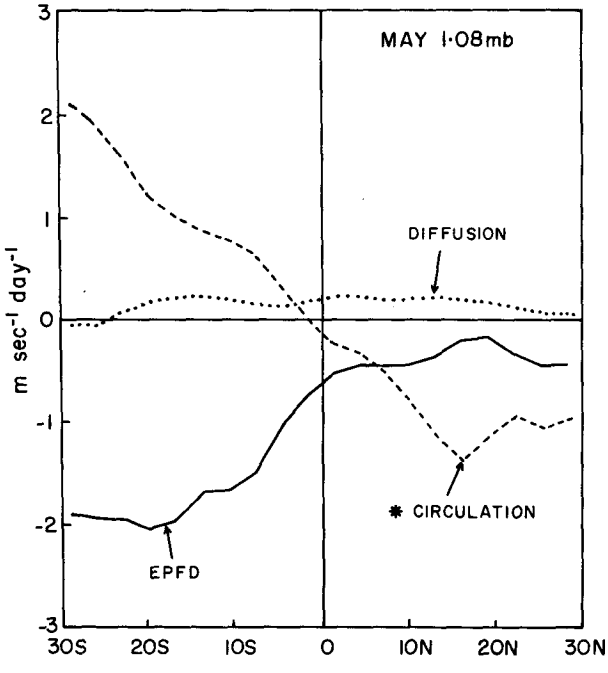

FIG. 14. As in Fig. 11, but for May.

The vertical/horizontal decompositions of the wave-driving in November and May are shown in Figs. 17 and 18. These reveal an easterly forcing from the horizontal component "eating into" the tropics from the autumn hemisphere. Once again, this component is much stronger in boreal autumn than in the austral autumn. The contribution to the mean flow forcing by the divergence of the vertical EP flux is small in both November and May.

The general pattern of the TE momentum balances seen at 1.08 mb is also found at all levels near the stratopause. As an example, Fig. 19 and 20 show the detailed TE balances for February at the 0.53 mb level. The westerly forcing from the vertical component of the EP flux has roughly the same meridional profile as

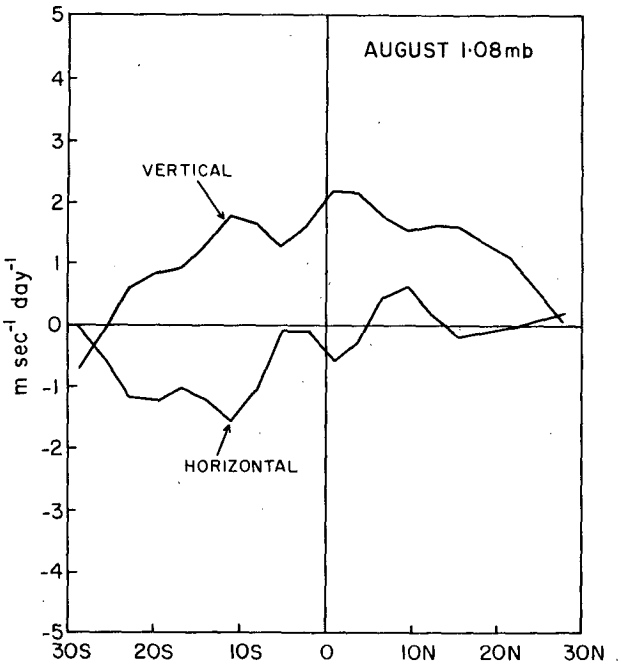

FIG. 16. As in Fig. 15, but for August.

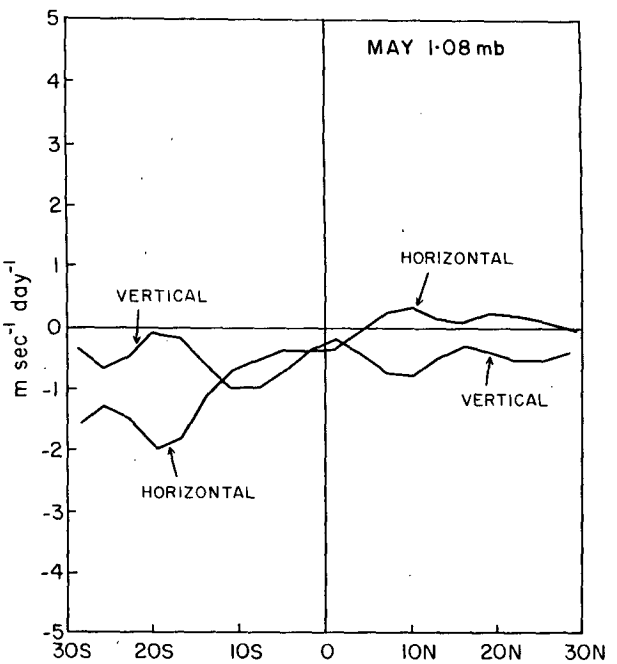

FIG. 18. As in Fig. 15, but for May.

at 1.08 mb, but is rather larger. However, the compensating easterly accelerations from the residual circulation are also larger at 0.53 mb than at 1.08 mb. This more complete cancellation means that the SAO actually decreases in amplitude above 1.08 mb, despite the larger westerly wave-driving at the higher levels.

6. Details of the wave-driving

The broad features seen in the TE diagnostics displayed in Figs. 11–20 appear, at least at first glance, to be consistent with earlier ideas concerning the forcing of the SAO. The westerly wave-driving is associated

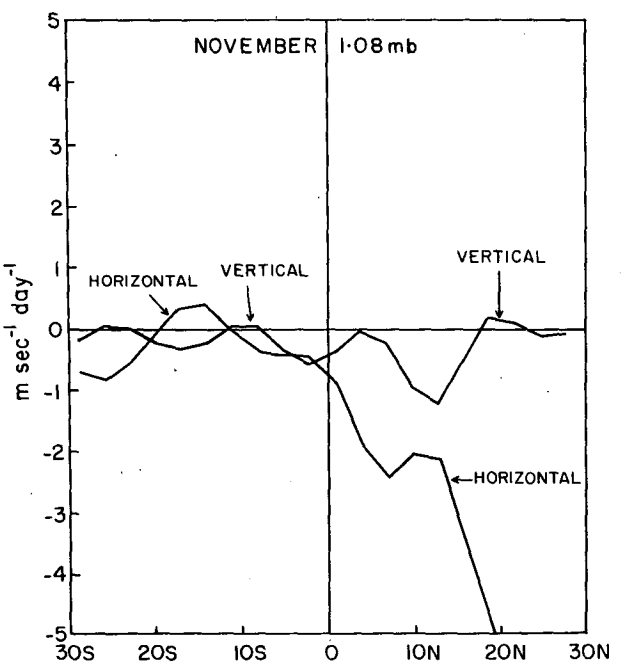

FIG. 17. As in Fig. 15, but for November.

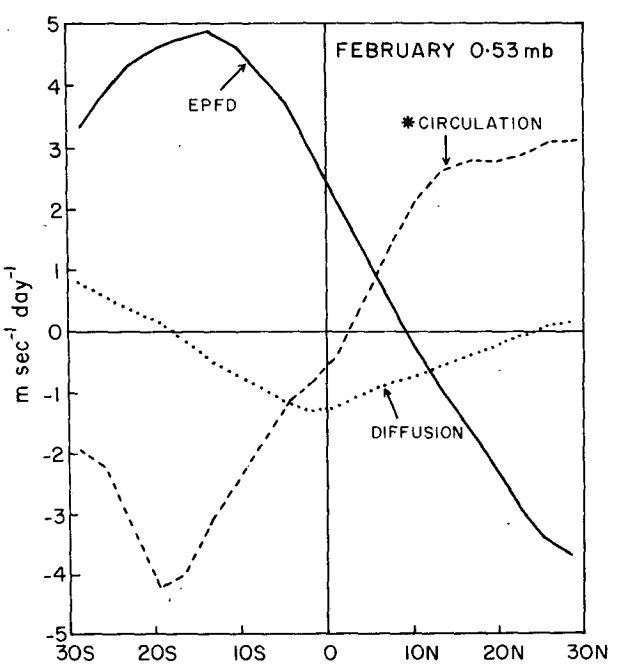

FIG. 19. As in Fig. 11, but for the 0.53 mb level.

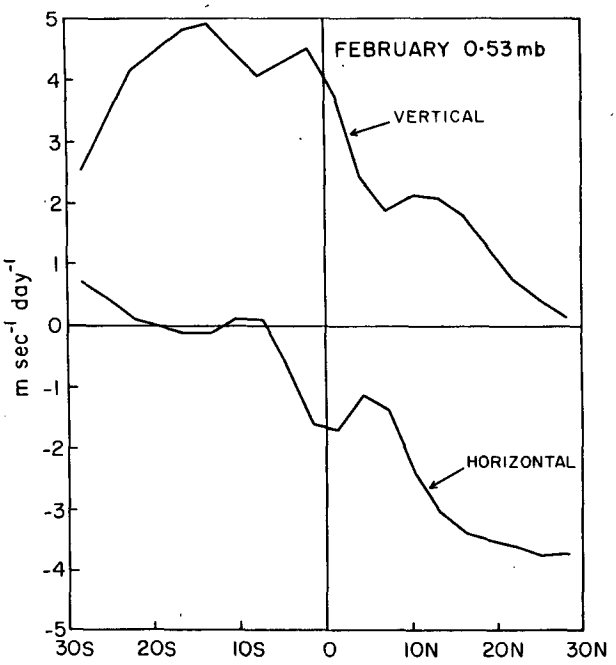

FIG. 20. As in Fig. 15, but for the 0.53 mb level.

only with the vertical EP flux and is equatorially trapped with a trapping width comparable to that anticipated for the 50–70 m s^{-1} Kelvin waves discovered by Hirota (1978). The easterly wave-driving comes from the horizontal EP flux, and has a meridional profile consistent with a simple view of how midlatitude planetary waves might be dissipated as they propagate from the winter hemisphere into the tropics. The detailed data available from the model simulation allow these interpretations to be more rigorously tested.

One fairly simple computation that can be performed is the decomposition of the EP flux divergence into different zonal wavenumbers. In the present project this was done for two 34-day segments of the period of high-frequency sampling during the "1983/84" winter (see last paragraph in section 3). The first of these segments was 15 December–17 January (i.e. during the easterly acceleration phase of the stratopause SAO), and the second was 8 February–12 March (during the westerly acceleration phase). The computation was performed by simply Fourier analyzing the fields around each latitude circle at each available time, and then reconstructing the variables including only a certain range of zonal wavenumbers. The reconstructed fields were then used to compute vertical and horizontal EP flux divergences.

The results for the horizontal EP flux divergence during 15 December–17 January at 1.08 mb are summarized in Fig. 21. This shows profiles of the wave-driving computed for zonal wavenumbers 1, wavenumbers 1 and 2, and for all wavenumbers (heavy curve). The results demonstrate that wavenumbers 1 and 2 account for nearly all the easterly wave-driving associated with the horizontal EP flux. This is consistent with the usual view that in the winter extratropics only wavenumbers 1 and 2 can effectively propagate into the upper stratosphere (e.g., Charney and Drazin 1961). Very similar results are obtained for the 8 February–12 March period (Fig. 22).

Figure 23 shows the same kind of analysis conducted for the vertical EP flux divergence during 15 December–17 January. The ranges of zonal wavenumber displayed are 1–5, 1–10, 1–20, and all wavenumbers (i.e., 1–50, heavy curve). The contrast with the results in Figs. 21 and 22 is striking. The wave-driving from the vertical component of EP flux is distributed rather evenly over a large range of zonal scales. The contribution from the planetary scales normally associated with the observed Kelvin waves (e.g., Hirota 1978; Salby et al. 1984) appears to be quite small. The same picture emerges from analysis of the simulated data during the 8 February–12 March period (Fig. 24).

The existence of a rich spectrum of vertically propagating gravity waves has been documented in earlier studies of the SKYHI GCM (Miyahara et al. 1986). The present results imply that the vertical momentum transport associated with these gravity waves is critical to the generation of the westerly phase of the SAO in the model. Preliminary results in a study of the 1° × 1.2° version of the model support this implica-

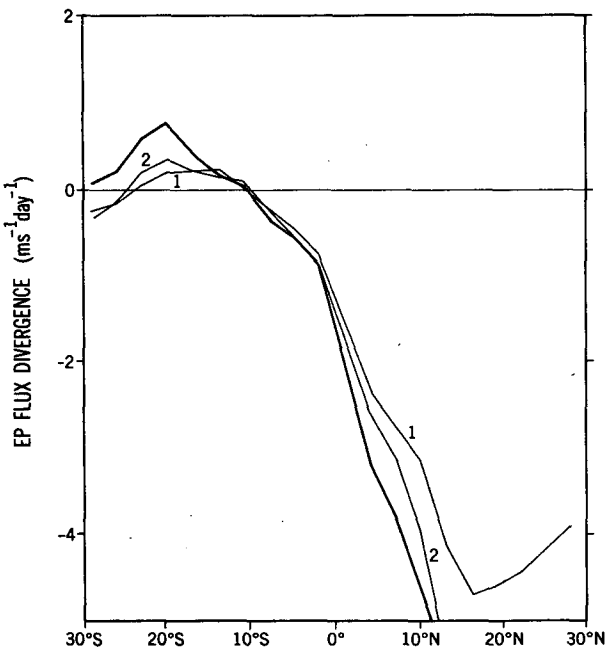

FIG. 21. The thick curve shows the total mean flow forcing from the divergence of the horizontal component of the EP flux during the period 15 December "1983" through 17 January "1984." The curve marked "1" is the same quantity computed when only zonal wavenumber one is considered. The curve labelled "2" shows the result when wavenumbers one and two are included.

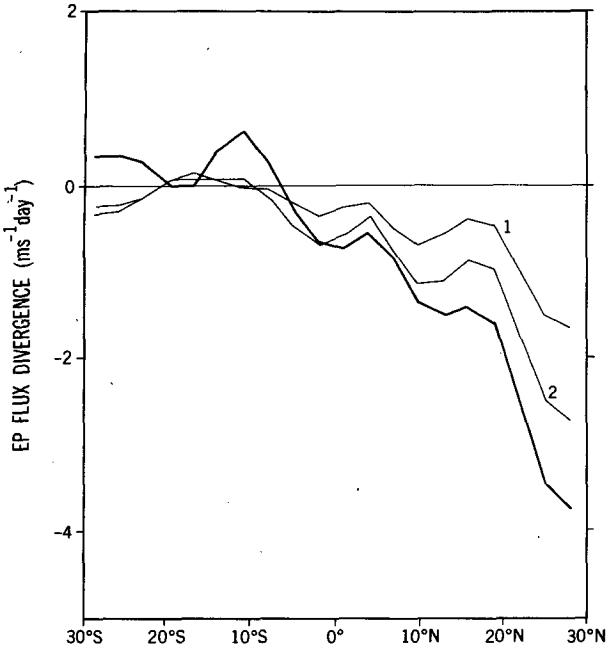

FIG. 22. As in Fig. 21, but for the period 8 February through 14 March "1984."

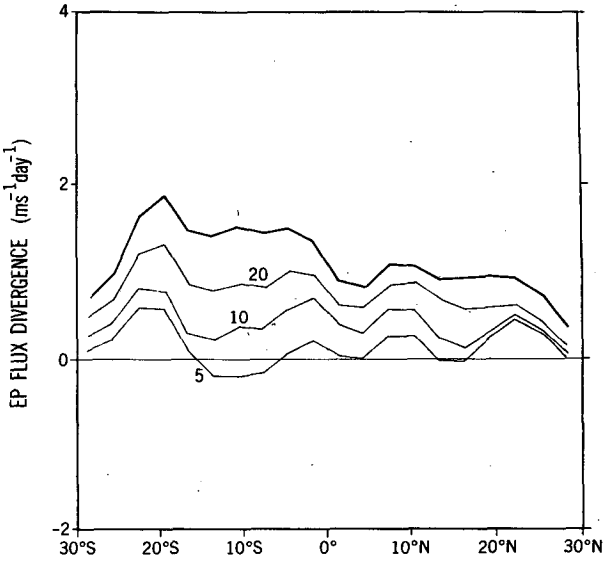

FIG. 23. The thick curve shows the total mean flow forcing from the divergence of the vertical component of the EP flux during the period 15 December "1983" through 17 January "1984." The curves marked "5," "10" and "20" show the same quantity computed when only zonal wavenumbers 1–5, 1–10 and 1–20 are included.

tion (Hayashi et al. 1988). In order to understand better the nature of this contribution to the wave-driving, space–time spectral analysis was applied to the simulated fields. The analysis was performed using the two-hourly snapshots saved during two eight-day periods: 15–22 December "1983" and 8–15 February "1984." The quantity actually computed was the cospectrum of the zonal velocity and the isobaric vertical velocity ω. Thus the result can be envisaged as a partitioning of the vertical eddy momentum flux into the various Fourier frequencies and zonal wavenumbers. The space–time periodogram was computed in the straightforward manner described by Hayashi (1971). In order to produce the spectral estimates shown below, the periodogram was smoothed by taking a running mean over five adjacent Fourier frequencies (i.e., a band-pass of 0.026 h^{-1}).

The results for 1.5°S during 8–15 February are shown in Figs. 25 and 26 for the 1.08 and 103 mb levels, respectively. The spectrum at 1.08 mb is quite similar to that seen at low latitudes in the earlier study of the SKYHI model by Miyahara et al. (1986). For the most part, waves with westerly (easterly) phase speeds are associated with vertical transport of westerly (easterly) momentum. For zonal wavenumbers 1–20 the activity for the westerly propagating waves tends to be concentrated in a band of zonal phase speeds centered around 55 m s^{-1}. As the zonal wavenumber increases above about 25, the dominant frequencies actually begin to decrease. As noted by Miyahara et al. (1986), this behavior is consistent with the existence of a spectrum of waves with varying zonal scales, but with a dominant vertical wavelength (~25 km at stratopause heights). For waves with horizontal wavelengths much larger than the numerical grid spacing, the usual gravity-wave dispersion relation would predict constant horizontal phase speeds for all components, i.e.

$$c = N/m$$

where c is the horizontal phase speed, m the vertical

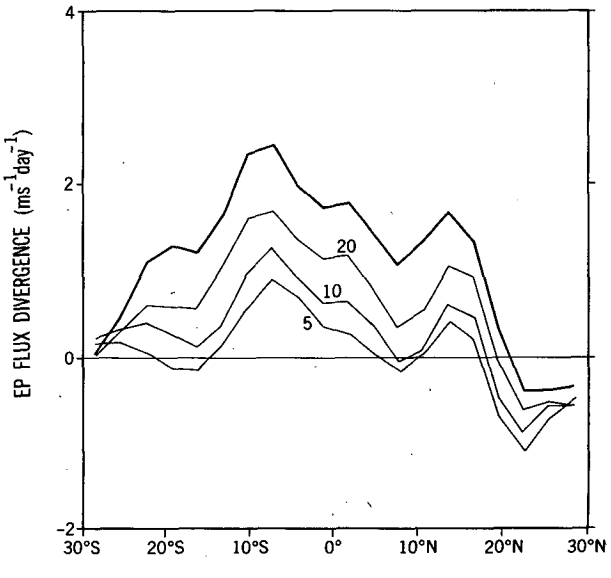

FIG. 24. As in Fig. 23, but for the period 8 February through 14 March "1984."

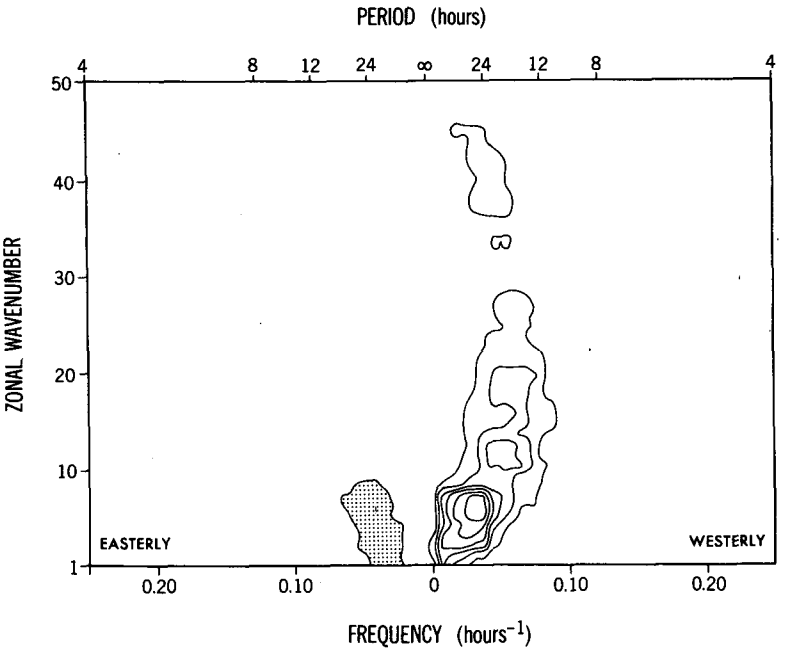

FIG. 25. Space–time cospectral density of the vertical eddy momentum flux $-u'\omega'$ at 1.5°S and the 1.08 mb level during 8 through 15 February "1984." The contour interval is 4×10^{-7} mb m s^{-2} day, but no zero contour is plotted. Negative values of magnitude larger than 4×10^{-7} have been shaded.

wavenumber, and N the Brunt–Väisälä frequency. However, those waves with horizontal scales comparable to the grid spacing will have frequencies significantly less than that predicted on the basis of the continuous gravity-wave dispersion relation.

The easterly propagating waves at 1.08 mb are weaker than the westerly waves. However, the general form of the distribution of the $\overline{u'\omega'}$ in the wavenumber–frequency domain for the easterly waves is actually rather similar to that found for the westerly waves (this is more apparent when Fig. 25 is replotted using a smaller contour interval). Given the dominance of the westerly waves at this level, it is not surprising that the net effect of the vertical EP flux in February (Fig. 22) is to produce a westerly mean flow forcing.

The results at 103 mb (Fig. 26) are similar to those shown in Fig. 25, but with a much larger fraction of the wave activity at lower frequencies. One odd feature of the results at this level is the concentration of power in easterly waves with horizontal wavelength very close to twice the grid spacing. There is no obvious explanation for this phenomenon. Fortunately, these very short wavelength waves tend to disappear very rapidly with height (presumably because of their very small frequencies), and thus they do not directly affect the simulation in the stratopause region.

From the space–time spectra it is straightforward to compute the total vertical momentum flux associated with all westerly waves or that associated with all easterly waves. In Fig. 27 these two quantities for the 8–15 February period are plotted as a function of latitude at the 103 mb level. The result shows that the wave fluxes for both the easterly and westerly waves emerging from the troposphere have an equatorially trapped structure. By the time the waves reach the stratopause (Fig. 28) the wave fluxes have been strongly reduced at all latitudes, but the reduction in the flux of easterly waves is more pronounced than that of the westerly waves. The maximum in the profile of the $\overline{u'\omega'}$ for the westerly waves is shifted significantly into the Southern Hemisphere relative to that seen at 103 mb. There also seems to be a slight shift into the Northern Hemisphere in the profile for the easterly waves.

The results shown in Figs. 24–28 can be fit into a consistent picture of the generation of the westerly forcing for the SAO in the model. At the stratopause level the accelerations are produced by waves with a broad spectrum of zonal scales and frequencies (Figs. 24 and 25). In fact most of the waves have horizontal scales sufficiently small and frequencies sufficiently large to regard them as "small scale" gravity waves (i.e., waves that are not significantly affected by the equatorial waveguide). In this case the equatorially trapped profile for the wave fluxes emerging from the troposphere (Fig. 27) must be attributed to a similar shape for the wave excitation. This, in turn, suggests moist convection as the dominant forcing mechanism for the vertically propagating waves in the tropics.

As the waves propagate vertically they will be subject to various dissipative effects. Radiative cooling acts on

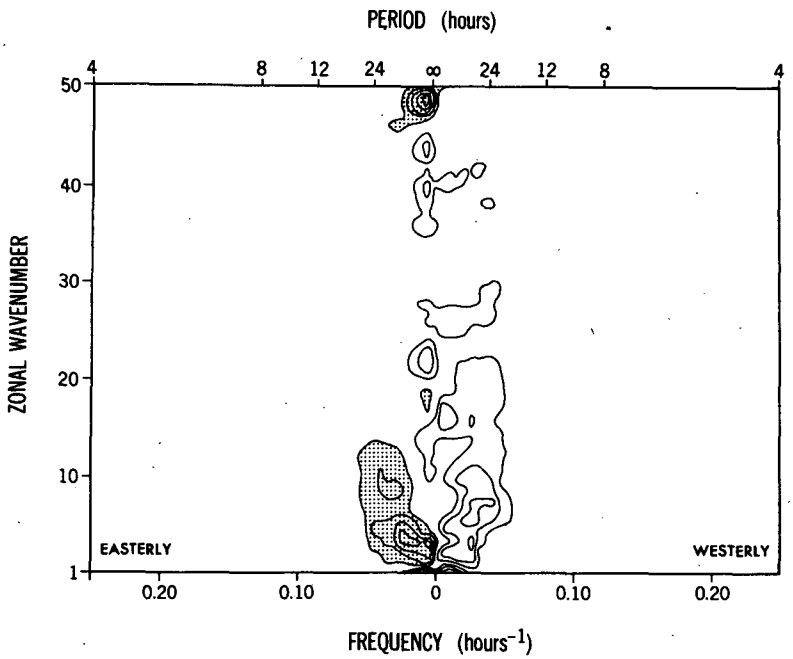

FIG. 26. As in Fig. 25, but for the 103 mb level. The contour interval is 8×10^{-6} mb m s^{-2} day.

time scales in the range of 5–50 days throughout most of the stratosphere (e.g., Fels 1982), and so is likely important only for the very low frequency waves seen in Figs. 25 and 26. The waves may also be dissipated by subgrid scale momentum and heat mixing in the model. In particular, the Richardson number-dependent vertical mixing is activated frequently during the model simulation. These vertical mixing events presumably provide an effective background viscosity for the whole spectrum of vertically propagating waves. The effects of such a viscosity will be stronger for those waves with shorter vertical wavelengths, i.e. smaller Doppler-shifted horizontal phase speeds (e.g., Matsuno 1982). The February mean $\bar{u}$ field for the model simulation (not shown) is reasonably similar to that in January (Fig. 2). It is easy to see that waves emerging above 100 mb will encounter mean easterlies throughout most of the tropical stratosphere. This may account for the enhancement of the ratio of the westerly-to-

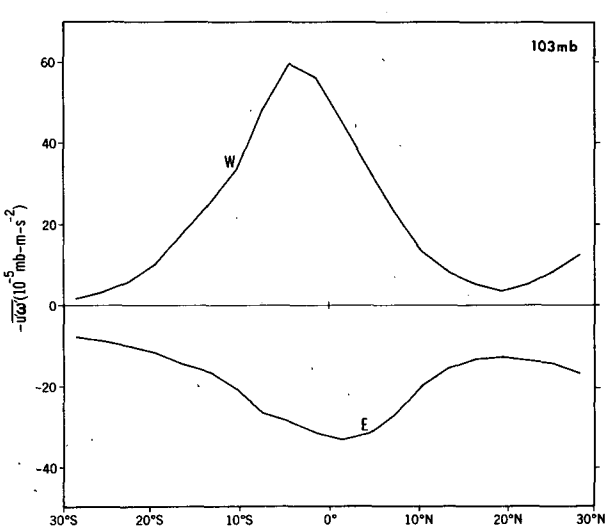

FIG. 27. Meridional profile of the total eddy vertical momentum flux associated with westerly-propagating waves (curve marked "W") and easterly-propagating waves (curve marked "E"). Results for 8–15 February at the 103 mb level.

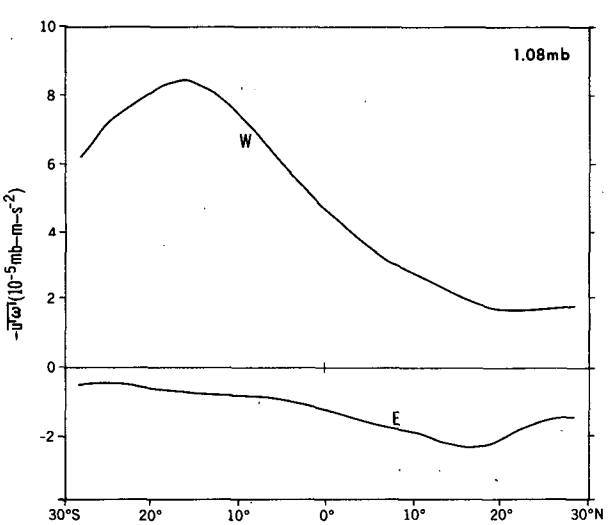

FIG. 28. As in Fig. 27, but for the 1.08 mb level.

easterly wave flux at 1.08 mb relative to that at 103 mb (Figs. 27 and 28). The horizontal gradient in the mean winds (westerly north of the equator, easterly south of the equator) may explain the fact that the enhancement of the westerly waves is more pronounced south of the equator.

Thus, the tendency for the peak in the meridional profile of westerly wave flux to move into the summer hemisphere (Figs. 25 and 26) can be understood if the waves are regarded as small-scale gravity waves unaffected by the equatorial waveguide, but subject to a vertical-scale-dependent dissipation. By contrast, the meridional profile of wave amplitude for a Kelvin mode in cross-equatorial shear like that seen in February should actually be peaked in the winter hemisphere (e.g., Boyd 1978).

The interpretation of the eddy motions in the tropical stratosphere as small-scale gravity waves, rather than as equatorially trapped waves, is supported by inspection of the raw fields produced during the model simulation. Figure 29 shows several snapshots of the eddy components (i.e. deviations from the zonal mean)

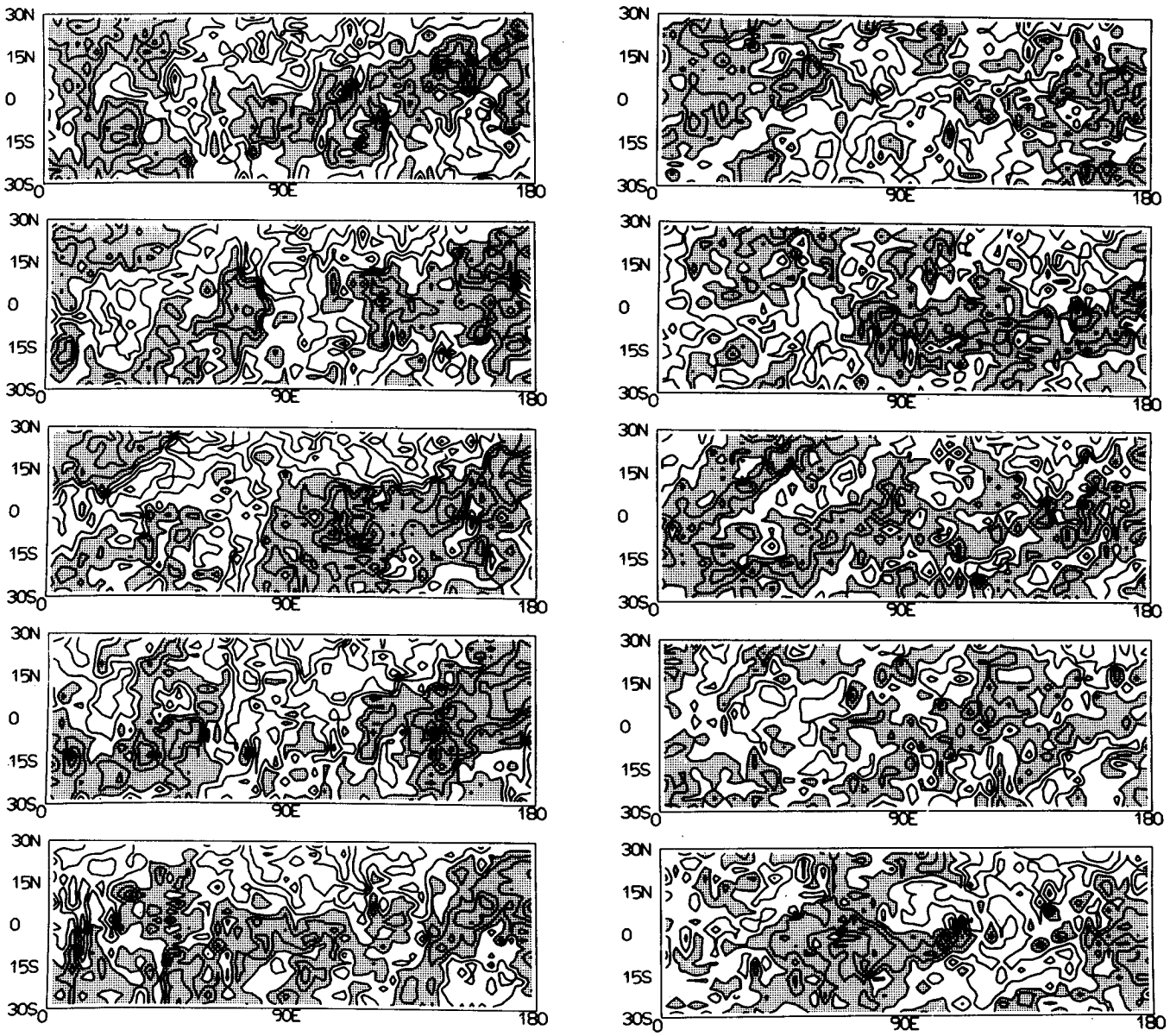

FIG. 29. The five panels on the left show instantaneous values of the eddy component of the zonal wind at 1.08 mb for five consecutive days, 15–19 December "1983." The right panels show the corresponding eddy meridional winds. The contour interval is 10 m s^{-1} and negative values are shaded. The maps are drawn so that the meridional and zonal coordinates are scaled correctly at 15° latitude.

of the zonal and meridional winds at the 1.08 mb level. Only the eastern hemisphere is shown and the projection was chosen so that the ratio of zonal to meridional scales is true at 15° latitude (and thus is close to being true over the full 30°S–30°N latitude band displayed). There is little indication of a significant tendency for dominant zonal propagation or dominant north–south orientation of phase lines. Indeed the wind fields in the snapshots look so complicated and chaotic that it is rather surprising that the space–time spectra reveal so much regularity in the wave fields.

The general pattern of gravity wave momentum fluxes discussed above for a period in February (i.e., during the westerly acceleration phase of the SAO) was also found in the analysis for 15–22 December "1983" (during the easterly mean flow acceleration). The principal difference in the December period is a smaller westerly/easterly momentum flux ratio at the stratopause. This can be seen in Fig. 30, which shows the meridional profiles of the vertical eddy momentum flux associated with easterly and westerly waves at 1.08 mb during 15–22 December. The difference from the February results (Fig. 28) may be due to the presence of somewhat weaker mean easterlies in the tropical middle and upper stratosphere in December than in February (there are actually weak mean westerlies at the equator in December between about 5 and 10 mb; see Fig. 6).

The *total* equatorial vertical eddy momentum flux, $-\overline{u'\omega'}$, in each month of the year is shown in Fig. 31 for both the 1.08 and 103 mb levels. The results display a small semiannual signal in the momentum flux emerging from the troposphere, with maximum westerly flux in February and July. However, there is a more pronounced annual cycle apparent, with the July maximum much stronger than that in February. It is not known how much of this seasonal variation in $\overline{u'\omega'}$ results from changes in the westerly/easterly flux ratio or from actual changes in the total wave activity.

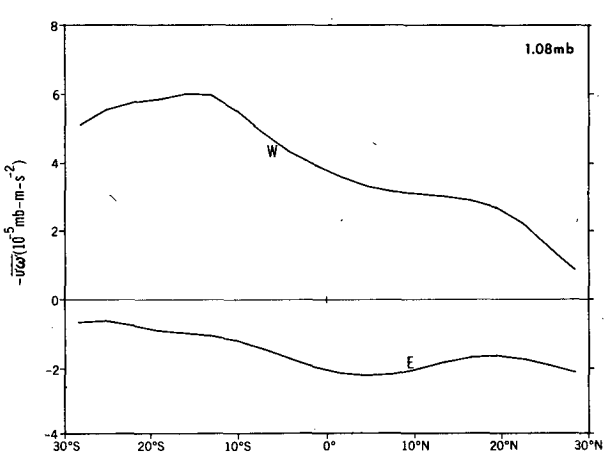

FIG. 30. As in Fig. 27, but for the 1.08 mb level during 15–22 December "1983."

The results shown in Fig. 31 for 1.08 mb are in sharp contrast to those at the tropopause. In particular, the semiannual modulation of the momentum flux is very pronounced. It thus appears that the semiannual character of the westerly wave-driving should be attributed primarily to the effects of wave dissipation and/or refraction in the stratosphere. In this sense at least, the present results may lend some support to models of the SAO which employ fixed eddy fluxes at the tropical tropopause (e.g., Dunkerton 1979; Takahashi 1984a,b).

Another interesting feature of Fig. 31 is the reversal of the phase of the annual cycle at 1.08 mb relative to that at 103 mb. At the stratopause the larger values of momentum flux (and hence presumably flux convergence) in January–February relative to July–August help balance the stronger easterly mean flow forcing associated with planetary waves in boreal winter (see Figs. 15 and 16).

The results discussed above suggest that large-scale Kelvin waves play a rather insignificant role in the momentum balance of the tropical stratopause region. It is natural to ask whether the model simulation really lacks the Kelvin waves seen in observational studies such as that of Salby et al. (1984). A detailed analysis of the large-scale equatorial waves in the model is beyond the scope of the present study. Hayashi et al. (1984) determined that the temperature variance attributable to wavenumber one Kelvin waves in the 5° × 6° version of the SKYHI model was roughly comparable to that found by Salby et al. A preliminary examination (Hayashi, private communication) suggest that the results in the 3° × 3.6° version are similar. Figure 32 shows a 34-day time series of the amplitude and phase of the zonal wavenumber one component of the temperature averaged at the four grid rows nearest the equator (4.5°S–4.5°N) at the 3.83 and 5.16 mb levels. This should be roughly comparable to the "equatorial" results presented for the 5 mb level in Fig. 3 of Salby et al. The model results display a predominant eastward propagation with a rather variable amplitude. Overall, Fig. 32 does resemble the comparable observations of Salby et al. although the model amplitude may be somewhat smaller than observed.

7. The simulated mesopause SAO

The 9° × 10° version of the SKYHI GCM produced a simulation of the equatorial winds that was dominated by a SAO nearly in-phase at all heights throughout the stratosphere and mesosphere (Mahlman and Sinclair 1980). This is a very unrealistic feature, since observations indicate a roughly 180° phase difference between the SAO at the mesopause and that at the stratopause (Hirota 1978; Hamilton 1982a). Mahlman and Umscheid (1984) discussed the simulation obtained with the 5° × 6° version of the model, and noted an improvement in the phase of the mesospheric

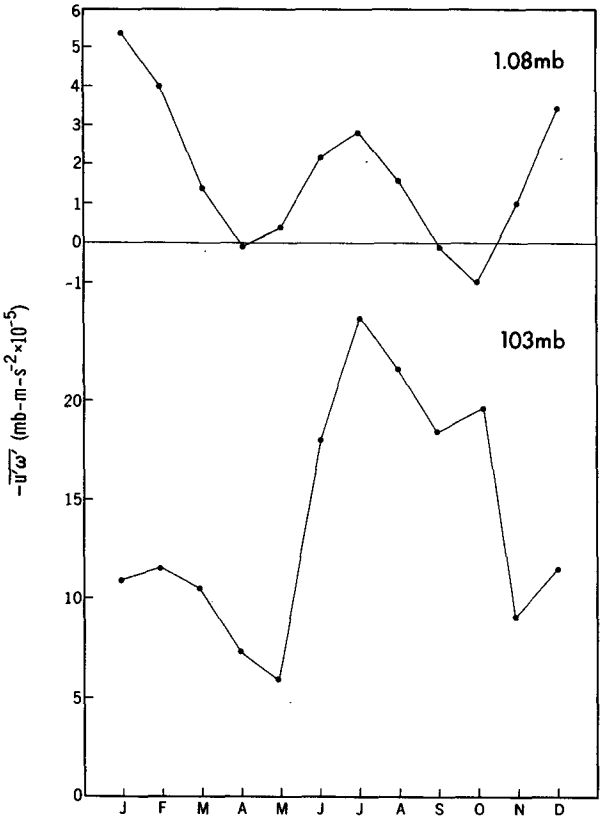

FIG. 31. Total vertical eddy momentum flux, $-u'\omega'$ for each month of the year at the equator (average of 1.5°N and 1.5°S). Results are shown for 1.08 mb (top) and 103 mb (bottom) and represent averages over the three years of model integration.

SAO. The present results for the 3° × 3.6° version of the model represent a further improvement in this regard (note the almost three month phase difference between 0.01 mb and 1 mb shown in Fig. 8). However, as discussed in section 4, the amplitude of the SAO near the mesopause even in the 3° × 3.6° model is less than one-half that actually observed.

The dynamics of the mesopause SAO as simulated in the GCM differ in some respects from those proposed by Dunkerton (1982). Dunkerton imagined that both easterly and westerly accelerations of the equatorial mean wind are driven by the EP flux divergences associated with vertically propagating waves. By contrast, in the model the effects of the residual circulation are implicated in the easterly acceleration phase. Figure 33 shows the components of the TE momentum balance at the 0.07 mb level (the third-highest level in the model) averaged over the three August months analyzed. The net easterly accelerations near the equator are due to the dominance of the momentum advection from the residual circulation over the westerly forcing from the EP flux divergence. The situation in the westerly acceleration phase is shown in Fig. 34 (TE balance at 0.07 mb in May). Here the westerly wave-driving at the equator dominates the combined effects of the residual circulation and the subgrid-scale momentum diffusion. The wave-driving (at least in the tropics) at these high levels is attributable almost entirely to the vertical component of the EP flux (presumably associated with vertically propagating gravity waves).

There are many possible causes for the unrealistically small amplitude of the mesospheric SAO in the model. One possibility is that the dissipation associated with the subgrid-scale mixing may be too strong and may simply act to damp the mean flow oscillation. The results in Figs. 33 and 34 show that (in contrast to the situation at the stratopause) the subgrid-scale mixing does play a very significant role in the zonal-mean momentum balance. Unfortunately, it is impossible to know whether the model's subgrid-scale mixing does represent a serious overestimate of the actual effects of small-scale turbulence at these heights.

Another potentially serious limitation of the model in the upper mesosphere is the imposition of a zero vertical velocity boundary condition at the top (see section 3). This may obviously affect the wave propagation through spurious downward reflection from the "lid." The upper boundary condition also acts as a constraint on the residual meridional circulation. The cross-equatorial flow associated with the residual circulation becomes very intensified at the top three model levels (particularly near the solstices when $\bar{v}^*$ at the equator can exceed 20 m s^{-1}). This may reflect the

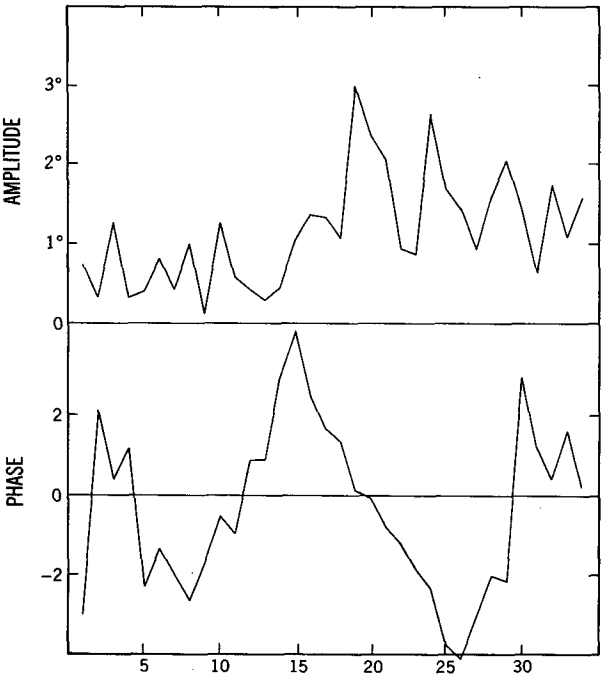

FIG. 32. Daily values of the amplitude (top) and phase (bottom) of the zonal wavenumber one component of temperature near 5 mb averaged between 4.5°N and 4.5°S. Negative slopes indicate eastward propagation with time and phase jumps of 2π are to be ignored.

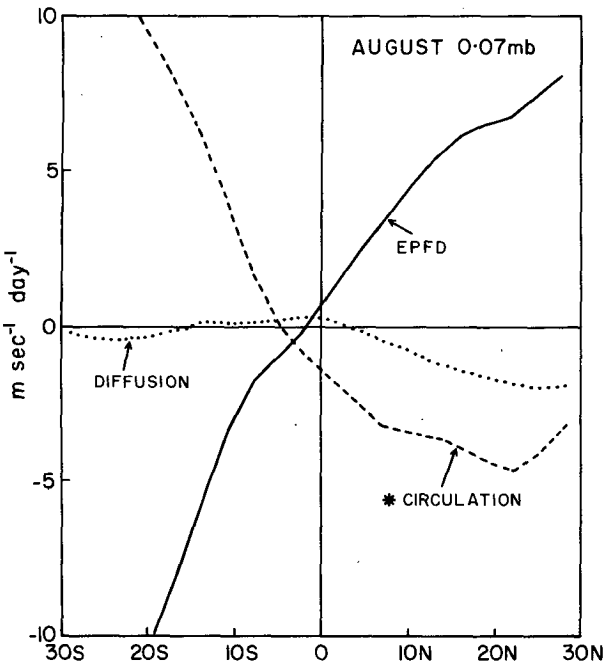

FIG. 33. As in Fig. 11, but for the 0.07 mb level in August.

fact that the rising (sinking) motions in the summer (winter) hemisphere are forced to abruptly stop at the model "lid."

Another obvious limitation of the model in the mesosphere is the coarse vertical resolution (note that over 6 km separate the top model level from the next highest). This could clearly affect the treatment of wave–mean flow interactions at these mesospheric heights.

A final concern in the mesospheric simulation is the omission of a diurnal radiative cycle in the model. The diurnal tide is thought to generate a strong easterly forcing of the mean flow near the tropical mesopause (Miyahara 1978a,b; Hamilton 1981). This may well account for the significant westerly bias seen in the simulated annual mean winds in the tropical upper mesosphere (see section 4). It is also possible that the rather poor simulation of the annual mean wind may contribute to the problems found in the model's mesopause SAO.

8. Simulation of the SAO in N_2O concentration

Jones and Pyle (1984) and Gray and Pyle (1986, 1987) studied satellite-retrieved values for the stratospheric concentration of N_2O and CH_4. These are long-lived trace constituents with strong vertical stratification in the stratosphere, and thus they should act as tracers of vertical air motion. A particularly interesting finding in these studies was a semiannual variation in the tracer concentrations in the tropical upper stratosphere. In particular, the N_2O and CH_4 mixing ratios in the upper stratosphere at the equator tend to be a minimum around April and October and maximum in January and July. Gray and Pyle (1986) suggested that this tracer SAO was connected directly to the dynamical SAO. In particular, the periods when there is westerly vertical shear at a particular level on the equator are also times of positive equatorial temperature anomalies in the SAO (consistent with thermal wind balance for the mean zonal wind). The warm temperatures should produce anomalous radiative cooling, and hence sinking of air parcels. Then the maximum downward displacement of the air parcels on the equator should occur when the descending westerly shear region has just passed, i.e., at the time of the maximum westerlies around April and October. Gray and Pyle (1987) showed that quite a realistic simulation of this effect could be obtained when a simple representation of a Kelvin wave-driving of the mean flow near the stratopause is included in a two-dimensional dynamical/chemical model.

Throughout the SKYHI model integration discussed in the present paper, the concentration of N_2O was carried as a predicted variable. The treatment of N_2O chemistry in the model was somewhat simplified, however. The N_2O field was initialized with realistic tropospheric values and then no new sources were included (a reasonable approach since the tropospheric N_2O lifetime is thought to be over a century (e.g., Levy et al. 1979). As the N_2O mixes into the stratosphere it is subject to photochemical destruction, which in the model is assigned a rate constant dependent on height and latitude, but not on season. The photochemical

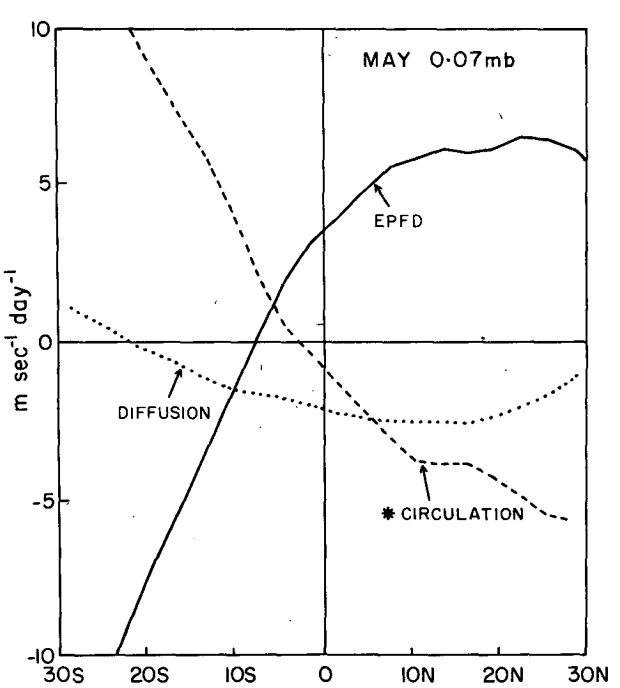

FIG. 34. As in Fig. 11, but for the 0.07 mb level in May.

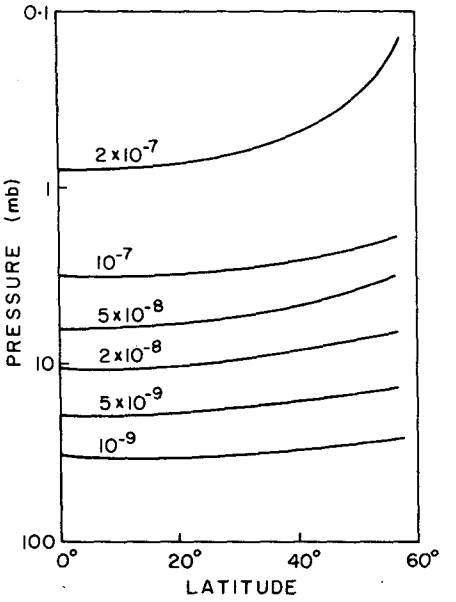

FIG. 35. Destruction rates used for the N_2O in the model simulation. Contour labels are in s^{-1}.

destruction rates used in the GCM are shown in Fig. 35. The use of annual-average destruction rates is clearly unrealistic in the high latitudes (where the real photochemical destruction must go to zero in the polar night), but may be reasonable in the tropics. The discussion below is confined to a brief look at how well the model reproduces the observed SAO in N_2O. Work is currently in progress to address the larger issues related to the global tracer transport in the model simulation.

The results obtained for the zonal mean N_2O climatology in January, April, July and October in the model are shown in Figs. 36–39. These can be compared to the satellite-derived observations shown in Fig. 1 of Gray and Pyle (1986). The overall pattern of the

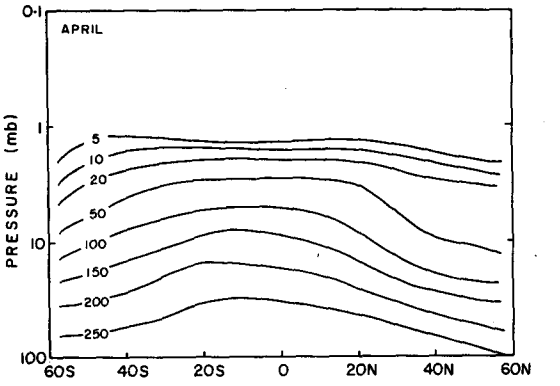

FIG. 37. As in Fig. 36, but for April.

N_2O isopleths is similar in the model and in observations, with a bulge (N_2O maximum) in the summer hemisphere in both January and July, and a "two-peaked" structure with an intervening equatorial minimum in April and October. The principal deficiency of the simulation lies in the failure to transport enough N_2O to upper stratospheric levels. For example, at 1 mb in January the model has less than 5 ppb of N_2O at any latitude, while the observations suggest that over 10 ppb are found at 1 mb. Similar discrepancies are apparent at other times of the year. It is encouraging to note that this problem is much less severe in the 3° × 3.6° model than in the lower-resolution versions (preliminary results suggest a further improvement in the 1° × 1.2° SKYHI model).

The seasonal variation of the equatorial N_2O values in the middle and upper stratosphere is in general agreement with the observational results in Gray and Pyle (1986). It is noteworthy, however, that the equatorial minimum in the model is more pronounced in October than in April, while the observations show the opposite interhemispheric asymmetry.

Given the simplicity of the "chemistry" employed,

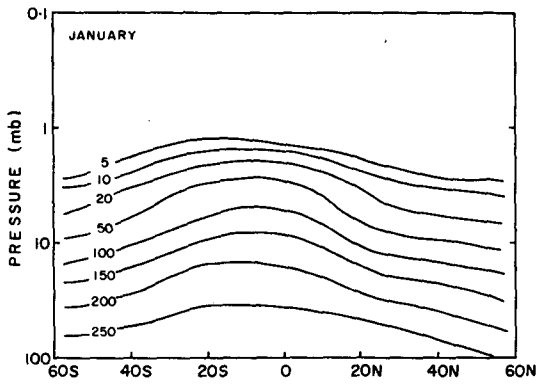

FIG. 36. Simulated zonal-mean N_2O concentrations averaged over three Januaries. Contour labels are in parts per billion by volume.

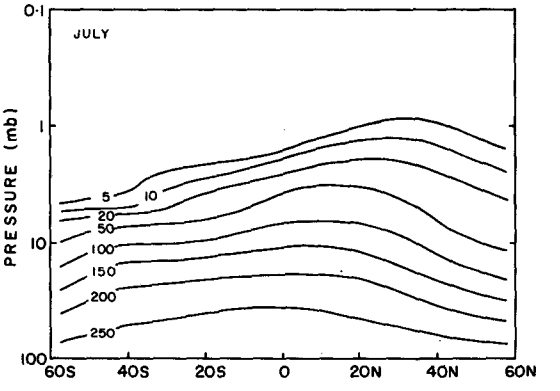

FIG. 38. As in Fig. 36, but for July.

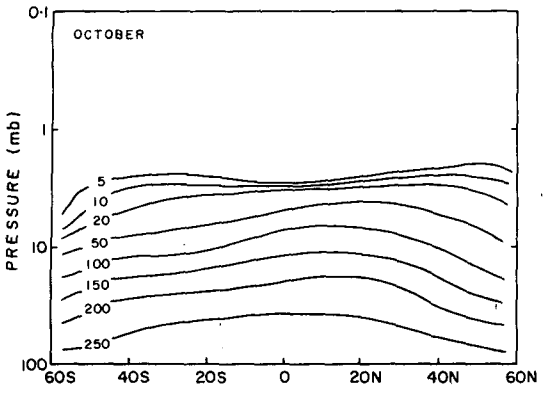

FIG. 39. As in Fig. 36, but for October.

it is clear that the SAO in equatorial N_2O values in the model must be attributed to dynamical effects. No detailed diagnosis of the mechanisms responsible has been attempted. However, it turns out that one quantity that can be easily computed is the contribution to the zonal mean N_2O budget from the transport due to the *Eulerian* meridional circulation. In Fig. 40 this quantity is plotted for each month of the year for the equator at 3.8 mb. This contribution is usually positive, presumably reflecting a general upward vertical velocity at the equator. However, it is modulated quite strongly by a semiannual cycle (minima in April and October). This is consistent with the mechanism advanced by Gray and Pyle (1986, 1987). Further work will be needed to elucidate other potentially important aspects of the tropical N_2O budget (such as transports from planetary waves), and to explain the difference between the equatorial N_2O fields seen in April and October.

9. Conclusion

The realistic simulation of the circulation in the tropical stratosphere and mesosphere represents a severe challenge for comprehensive GCMs. Adequate simulation of the mean zonal flow in the tropical middle atmosphere may well require realistic representations of (i) the generation of both tropical and extratropical planetary-scale waves, (ii) the vertical and horizontal propagation of such waves and their interaction with the mean flow, (iii) the generation and absorption of smaller-scale gravity waves, and (iv) the cross-equatorial flow associated with the residual meridional circulation (which will depend on the radiative heating rates throughout the global atmosphere). Given all the different kinds of dynamical processes that may be involved, it is encouraging to see that the 3° × 3.6° 40-level SKYHI model has been able to produce a simulation that is realistic in some important respects. In particular, the mean flow evolution near the tropical stratopause is dominated by a SAO of realistic amplitude, phase, and meridional width. The flow in the upper mesosphere in the model displays a SAO which has the correct phase (although with a weaker amplitude than actually observed). It is encouraging that these desirable features of the simulation (especially the width of the stratopause SAO and the phase of the mesospheric SAO) have improved considerably with increasing horizontal resolution in the model.

There are also some disappointing aspects to the SKYHI simulation described here. Most notable is the absence of a quasi-biennial oscillation in the tropical lower stratosphere. In addition, the detailed vertical structure of the stratopause SAO has the unrealistic feature of a gradual downward propagation of the easterly acceleration phase. Finally, the annual-mean zonal winds in the tropical upper mesosphere are quite unrealistic in the model (simulated westerlies rather than the strong easterlies actually observed).

The rather good simulation of the stratopause SAO encouraged a further investigation of the detailed dynamics of this phenomenon. The results show clearly that the easterly accelerations are to be attributed largely to the effects of the residual circulation in the summer hemisphere, and to the effects of horizontal EP fluxes from planetary-scale waves in the winter hemisphere, as indicated earlier by Mahlman and Umscheid (1984). The westerly mean flow accelerations are forced by a vertical EP flux convergence with an equatorially trapped profile. While this profile looks superficially like that anticipated for a large-scale Kelvin wave, the actual EP flux is distributed over a very broad spectrum of zonal scales and frequencies. Much of the wave activity is in quite high frequency waves (periods of less than one day) that may not be strongly influenced by the equatorial waveguide. Thus it may

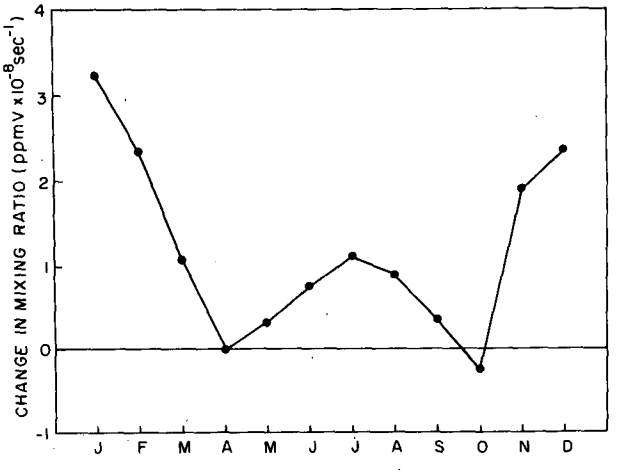

FIG. 40. Contribution to the rate of change in zonal-mean N_2O mixing ratio at the equator (average of 1.5°S and 1.5°N) due to transport by the Eulerian mean meridional circulation at the 3.8 mb level in the model. Results are plotted for each month of the year and are connected by straight lines. Each dot represents an average for a three year climatology.

be most appropriate to regard the westerly mean-flow forcing as resulting from dissipation of a wide spectrum of vertically-propagating gravity waves. Hitchmann and Leovy (1988) estimated that large-scale Kelvin waves (zonal wavenumbers 1–3) actually account for between 20% and 70% of the westerly EP flux convergence near the equatorial stratopause. The present results might be reconciled with the 20% figure, but clearly disagree with any higher estimate of the Kelvin wave forcing. It must be noted, however, that the results of Hitchmann and Leovy are based on a rather indirect analysis. For example, they estimate the Kelvin wave EP fluxes from the observed temperature variance in certain wavenumber–frequency ranges.

The diagnostic analyses described in sections 5 and 6 have led to a fairly complete picture of how the stratopause SAO operates in the GCM. There remain aspects of the simulation that should be investigated further, however. In particular, the processes involved in the generation and dissipation of gravity waves in the model need to be elucidated.

While it is a reasonably straightforward matter to diagnose the mechanical processes in the GCM, it is more difficult to determine the relevance of the detailed dynamics in the model to the real SAO. However, it is possible at least to speculate on how the SAO in the real atmosphere might differ from that documented in the SKYHI model. In particular, the principal deficiency in the overall model simulation is the tendency to be too close to radiative equilibrium in the stratosphere and mesosphere. This presumably results in radiative heating/cooling rates of too small a magnitude in both winter and summer hemispheres. This, in turn, should lead to a simulation with an unrealistically small cross-equatorial residual flow. It is possible that this could result in an underprediction of the effects of the residual circulation in generating the easterly phase of the SAO. If this is the case, then presumably the planetary wave effects will be less important for generating the easterly accelerations in the real atmosphere than in the model. It is thus tempting to speculate that in the model the planetary wave flux tends to be refracted more into the tropics than in the real atmosphere. This would result in enhanced local easterly wave-driving in the tropics and might also account (at least in part) for the tendency of the waves in the model extratropics to be too weak (and hence for the global stratospheric temperature structure to be too close to radiative equilibrium).

It is also possible that the model might misrepresent the cause of the westerly SAO acceleration, of course. Indeed if the results of Hitchman and Leovy (1988) are correct, then the model may produce a simulation in which too small a fraction of the vertical momentum flux in the tropics is concentrated in planetary-scale Kelvin waves. On the other hand, it is clear that the $3° \times 3.6°$ model does not include any momentum fluxes from gravity waves with horizontal wavelengths less than about 600 km (and probably significantly misrepresents those waves with wavelengths shorter than about 1200 km). It is quite possible that in the real atmosphere these smaller-scale waves could play an important role in the dynamics of the SAO.

Another interesting question is how the model simulation of the SAO would be affected if the model had a realistic QBO in the lower stratosphere. In particular, the dominance of westerly over easterly-propagating waves at the equatorial stratopause (e.g., Fig. 28) might not be so pronounced during the period when the lower stratosphere was filled with mean westerlies. This would presumably reduce the westerly accelerations in the SAO.

The present work is now being extended at GFDL through further detailed analysis of the existing simulation, and through new model developments. The simulation is being examined to determine the detailed forcing and dissipation mechanisms of the gravity waves in the model. Another project involves the verification of the statistical features of the high-frequency/small-scale wind and temperature fields in the GCM against historical rocketsonde and lidar observations. Such a study could aid in assessing the credibility of the model results concerning the spectrum of vertical eddy momentum fluxes.

The SKYHI model is also being extended and developed in various ways. Given the improvement in the SAO simulation in the $3° \times 3.6°$ model over earlier lower-resolution versions, it is reasonable to attempt a further increase in horizontal resolution. A $1° \times 1.2°$ version of the SKYHI model is now running. However, it will be several years before even a single model year of simulation will be available. Another project in progress involves a significant increase in vertical resolution, along with an extension of the model domain into the lower thermosphere. This version of the model will also include diurnal tides. The hope is that this model may produce a better simulation of both the annual mean wind structure and the SAO in the mesosphere. It is also possible that an increase in the vertical resolution in the tropical lower stratosphere could allow the model to better represent the wave–mean flow process for slow phase speed (i.e., short vertical wavelength) gravity and equatorial waves. It is conceivable that this might lead to the appearance of a quasi-biennial oscillation in the model (or at least some more interesting time-dependence to the mean winds in the tropical lower stratosphere).

Finally, it is worthwhile emphasizing that numerical models, no matter how sophisticated, can provide only limited insights into the behavior of the real atmosphere. Definitive understanding of the dynamics of the SAO will require acquisition of more observational data. A very useful contribution could be made by the installation of MST radars at one or more tropical lo-

cations. It is also to be hoped that further advances in satellite-based remote sensing will lead to a more detailed observational picture of the SAO.

Acknowledgments. The authors wish to thank L. Umscheid for his work in developing the model code and performing the integration employed in this work. They are also grateful for the helpful comments of S. Fels, Y. Hayashi, C. Leovy, H. Kida and an anonymous referee.

REFERENCES

Andrews, D. G., J. D. Mahlman and R. W. Sinclair, 1983: Eliassen-Palm diagnostics of wave-mean flow interaction in the GFDL "SKYHI" general circulation model. *J. Atmos. Sci.*, **40**, 2768–2784.

Angell, J. K., and J. Korshover, 1970: Quasi-biennial, annual and semiannual zonal wind and temperature harmonic amplitudes and phases in the stratosphere and low mesosphere of the Northern Hemisphere. *J. Geophys. Res.*, **75**, 543–550.

Barnett, J. J., and M. Corney, 1985: Middle atmosphere reference model. *Middle Atmosphere Handbook*, **16**, 47–85.

——, —— and K. Labitzke, 1985: Annual and semiannual cycles based on the middle atmosphere reference model. *Middle Atmos. Handbook*, **16**, 175–180.

Belmont, A. D., G. D. Dartt and G. D. Nastrom, 1974: Periodic variations in stratospheric zonal wind from 20 to 65 km at 80 degrees North to 70 degrees South. *Quart. J. Roy. Meteor. Soc.*, **100**, 208–211.

Boyd, J. P., 1978: The effects of latitudinal shear on equatorial waves, Part II: Application to the atmosphere. *J. Atmos. Sci.*, **35**, 2259–2267.

Cayford, J., and K. Hamilton, 1987: Monthly mean wind and temperature climatologies based on rocket soundings from 20 meteorological rocket stations throughout the world. McGill University Climate Research Group Report No. 87-5, McGill University, 44 pp. [Available from Department of Meteorology, McGill University, 805 Sherbrooke St. W., Montreal, Canada H3A 2K6.]

Charney, J. G., and P. G. Drazin, 1961: Propagation of planetary-scale disturbances from the lower into the upper atmosphere. *J. Geophys. Res.*, **66**, 83–109.

CIRA, 1972: *The COSPAR International Reference Atmosphere*, Akademie-Verlag, 450 pp.

Delisi, D. P., and T. J. Dunkerton, 1988: Seasonal variation of the semiannual oscillation. *J. Atmos. Sci.*, in press.

Dunkerton, T. J., 1979: On the role of the Kelvin wave in the westerly acceleration phase of the semiannual zonal wind oscillation. *J. Atmos. Sci.*, **36**, 32–41.

——, 1982: Theory of the mesopause semiannual oscillation. *J. Atmos. Sci.*, **39**, 2681–2690.

——, 1985: A two-dimensional model of the quasi-biennial oscillation. *J. Atmos. Sci.*, **42**, 1151–1160.

Fels, S. B., 1982: A parameterization of scale-dependent radiative damping rates in the middle atmosphere. *J. Atmos. Sci.*, **39**, 1141–1152.

——, J. D. Mahlman, M. D. Schwarzkopf and R. W. Sinclair, 1980: Stratospheric sensitivity to perturbations in ozone and carbon dioxide: Radiative and dynamical response. *J. Atmos. Sci.*, **38**, 2265–2297.

Gao, X. H., W. B. Yu and J. L. Stanford, 1987: Global features of the semi-annual oscillation in stratospheric temperatures and comparisons between seasons and hemispheres. *J. Atmos. Sci.*, **44**, 1041–1048.

Gray, L. J., and J. A. Pyle, 1986: The semi-annual oscillation and equatorial tracer distributions. *Quart. J. Roy. Meteor. Soc.*, **112**, 387–407.

——, and ——, 1987: Two-dimensional model studies of equatorial dynamics and tracer distributions. *Quart. J. Roy. Meteor. Soc.*, **113**, 637–654.

Geller, M. A., M.-F. Wu and M. E. Gelman, 1983: Troposphere–stratosphere (surface-55 km) monthly winter general circulation statistics for the Northern Hemisphere—four year averages. *J. Atmos. Sci.*, **40**, 1334–1352.

Hamilton, K., 1981: Numerical studies of wave–mean flow interaction in the stratosphere, mesosphere and lower thermosphere. Ph.D. thesis, Princeton University, 384 pp.

——, 1982a: Rocketsonde observations of the mesospheric semi-annual oscillation at Kwajalein. *Atmos.-Ocean*, **20**, 281–286.

——, 1982b: Some features of the climatology of the Northern Hemisphere stratosphere revealed by NMC upper atmosphere analyses. *J. Atmos. Sci.*, **39**, 2737–2749.

——, 1982c: Stratospheric circulation statistics. National Center for Atmospheric Research Tech. Note TN-191+STR, 174 pp. [Available from Publications Office, NCAR, P.O. Box 3000, Boulder, Colorado 80307.]

——, 1986: Dynamics of the stratospheric semiannual oscillation. *J. Meteor. Soc. Japan*, **64**, 227–244.

Hayashi, Y., 1971: A generalized method of resolving disturbances into progressive and retrogressive waves by space Fourier and time cross-sectral analysis. *J. Meteor. Soc. Japan*, **49**, 125–128.

——, D. G. Golder and J. D. Mahlman, 1984: Stratospheric and mesospheric Kelvin waves simulated by the "SKYHI" general circulation model. *J. Atmos. Sci.*, **41**, 1971–1984.

——, ——, —— and S. Miyahara, 1988: The effect of horizontal resolution on gravity waves simulated by the GFDL "SKYHI" general circulation model. *Pure Appl. Geophys.*, in press.

Hirota, I., 1978: Equatorial waves in the upper stratosphere and mesosphere in relation to the semiannual oscillation of the zonal wind. *J. Atmos. Sci.*, **35**, 714–722.

——, 1980: Observational evidence of the semiannual oscillation in the tropical middle atmosphere. *Pure Appl. Geophys.*, **118**, 217–238.

Hitchman, M. H., and C. B. Leovy, 1986: Evolution of the zonal mean state in the equatorial middle atmosphere. *J. Atmos. Sci.*, **43**, 3159–3176.

——, and ——, 1988: Estimation of the Kelvin wave contribution to the semiannual oscillation. *J. Atmos. Sci.*, in press.

Holton, J. R., 1975: *The Dynamical Meteorology of the Stratosphere and Mesosphere, Meteor. Monogr.*, **15**, No. 37, 216 pp.

——, and W. M. Wehrbein, 1980: A numerical model of the zonal mean circulation of the middle atmosphere. *Pure Appl. Geophys.*, **118**, 284–306.

Hopkins, R. H., 1975: Evidence of polar-tropical coupling in upper stratospheric zonal winds. *J. Atmos. Sci.*, **32**, 712–719.

Jones, R. L., and J. A. Pyle, 1984: Observations of CH_4 and N_2O by the NIMBUS 7 SAMS: A comparison of *in situ* data and two-dimensional numerical model calculations. *J. Geophys. Res.*, **89**, 5263–5279.

Levy II, H., J. D. Mahlman and W. J. Moxim, 1979: A preliminary report on the numerical simulation of the three-dimensional structure and variability of atmospheric N_2O. *Geophys. Res. Lett.*, **6**, 155–158.

Mahlman, J. D., and R. W. Sinclair, 1980: Recent results from the GFDL troposphere–stratosphere–mesosphere general circulation model. *Collection of Extended Abstracts Presented at ICMUA Sessions and IUGG Symposium 18*, IAMAP, Boulder, 11–18. [Available from S. Ruttenburg, UCAR, P.O. Box 3000, Boulder, Colorado 80307.]

——, and L. J. Umscheid, 1984: Dynamics of the middle atmosphere: Successes and problems of the GFDL "SKYHI" general circulation model. *Dynamics of the Middle Atmosphere*, J. R. Holton and T. Matsuno, Eds., Terra Scientific, 501–525.

——, and ——, 1987: Comprehensive modeling of the middle atmosphere: The influence of horizontal resolution. *Transport Processes in the Middle Atmosphere*, G. Visconti and R. Garcia, Eds., D. Riedel, 251–266.

Matsuno, T., 1982: A quasi one-dimensional model of the middle atmosphere circulation interacting with internal gravity waves. *J. Meteor. Soc. Japan,* **60,** 215–226.

Meyer, W. D., 1970: A diagnostic numerical study of the semiannual variation of the zonal mean wind in the tropical stratosphere and mesosphere. *J. Atmos. Sci.,* **27,** 820–830.

Miyahara, S., 1978a: Zonal mean winds induced by vertically propagating atmospheric tidal waves in the lower thermosphere, Part I. *J. Meteor. Soc. Japan,* **56,** 86–97.

——, 1978b: Zonal mean winds induced by vertically propagating atmospheric tidal waves in the lower thermosphere, Part II. *J. Meteor. Soc. Japan,* **56,** 548–558.

——, Y. Hayashi and J. D. Mahlman, 1986: Interactions between gravity waves and the planetary-scale flow simulated by the GFDL "SKYHI" general circulation model. *J. Atmos. Sci.,* **43,** 1844–1861.

Murgatroyd, R. A., 1969: The structure and dynamics of the stratosphere. *The Global Circulation of the Atmosphere,* G. A. Corby, Ed., Roy. Meteor. Soc., 159–195.

Plumb, R. A., 1977: The interaction of two internal gravity waves with the mean flow: Implications for the theory of the quasi-biennial oscillation. *J. Atmos. Sci.,* **34,** 1847–1858.

——, and R. C. Bell, 1982: A model of the quasi-biennial oscillation on an equatorial beta-plane. *Quart. J. Roy. Meteor. Soc.,* **108,** 335–352.

Reed, R. J., 1965: The quasi-biennial oscillation of the atmosphere between 30 and 50 km over Ascension Island. *J. Atmos. Sci.,* **22,** 331–333.

——, 1966: Zonal wind behavior in the equatorial stratosphere and lower mesosphere. *J. Geophys. Res.,* **71,** 4223–4233.

Salby, M. L., D. L. Hartmann, P. L. Bailey and J. C. Gille, 1984: Evidence for equatorial Kelvin modes in Nimbus 7 LIMS. *J. Atmos. Sci.,* **41,** 220–235.

Takahashi, M., 1984a: A two-dimensional numerical model of the semi-annual zonal wind oscillation. *Dynamics of the Middle Atmosphere,* J. R. Holton and T. Matsuno, Eds., Terra Scientific, 253–269.

——, 1984b: A numerical model of the semi-annual oscillation. *J. Meteor. Soc. Japan,* **62,** 52–68.